Properties of strained wurtzite GaN and AlN: *Ab initio* studies

J.-M. Wagner and F. Bechstedt
Institut für Festkörpertheorie und Theoretische Optik, Friedrich-Schiller-Universität, 07743 Jena, Germany
(Received 30 November 2001; revised manuscript received 4 March 2002; published 10 September 2002)

The structural, dielectric, lattice-dynamical, and electronic properties of biaxially and uniaxially strained group-III nitrides are studied *ab initio* using a pseudopotential-plane-wave method. A linear-response approach to the density-functional theory is used to calculate the dielectric constants, the dynamical effective charges, and the phonon frequencies. For a given strain the atomic coordinates are determined from the equilibrium condition. The elastic properties of GaN and AlN are characterized in terms of ratios of the elastic stiffness constants, which allow for a critical comparison with literature data; unreliable ones are pointed out. Electronic as well as phonon deformation potentials and the respective strain and stress coefficients are determined. We show that the quasicubic approximation does not hold for the electronic interband deformation potentials of GaN but for those of AlN. Seeming discrepancies between experimental and theoretical results can be widely resolved using suitable parameters and correct stress-strain relations. We find that the stress obtained from biaxial-strain-induced shifts of the high-frequency E_2 phonon or excitonic transitions should be higher than determined by other authors.

DOI: 10.1103/PhysRevB.66.115202 PACS number(s): 63.20.−e, 62.20.Dc, 71.20.Nr, 77.22.Ch

I. INTRODUCTION

An important problem in growing GaN and AlN layers on crystalline substrates like, e.g., sapphire, SiC, ZnO, Si, or GaAs, is related to the large lattice mismatch and the difference in the thermal-expansion coefficients between epitaxial layer and substrate. They can cause large biaxial stresses in the epitaxial layers. For instance, such a stress is compressive for hexagonal GaN grown on sapphire, or tensile for GaN on 6*H*-SiC.[1–3] The situation is more complex in the case of GaN/AlN heterostructures or superlattices, where a mutual influence of the different material layers may occur.[4,5]

Whereas investigations of strain effects have been widely reported for the electronic and optical properties,[2–4,6–9] much less is known about their influence on the lattice-dynamical properties and the electron-phonon interaction. The Fröhlich coupling of longitudinal-optical (LO) phonons to electrons is governed both by the high-frequency and the static dielectric constant.[10] According to the Lyddane-Sachs-Teller relation, the latter is related to the former by the zone-center LO-phonon and transverse-optical (TO) phonon frequency. There were only a few Raman studies of the optical phonons under biaxial strain which are accompanied by a determination of the phonon deformation potentials in GaN (Refs. 7 and 11) [without covering the E_1(LO) mode] or of the strain and stress coefficient for the high-frequency E_2 mode of GaN (Refs. 12–14) and AlN,[15] by the investigation of carrier concentrations in GaN,[16] or by the study of stress and strain in the vicinity of cracks in AlN.[17]

Shifted phonon frequencies are straightforward signatures of the strain state of a layer. The shift coefficients are commonly also used to infer the stress state from Raman experiments, especially from micro-Raman investigations.[18] Besides the use of a reference value for the unshifted phonon frequencies, this requires a knowledge of the elastic properties of the material under consideration. On the other hand, there are still considerable uncertainties concerning the values of the elastic constants and of related quantities for the wurtzite nitrides. Moreover, there is a variety of contradictory data for the stress coefficient of the high-frequency E_2 mode of GaN. Therefore, a consistent description of the elastic properties and of the strain and stress dependence of the phonon frequencies as well as of the dielectric properties of wurtzite GaN and AlN is highly desirable.

In this paper, we present *ab initio* studies of the influence of biaxial and of uniaxial strain on the atomic structure as well as on the accompanying physical properties of wurtzite GaN and AlN as examples of group-III nitrides. Biaxial strain is considered due to lattice mismatch or thermal strain during epitaxial growth, whereas uniaxial strain could be a consequence of an applied external uniaxial pressure. We focus on the elastic properties of wurtzite GaN and AlN by describing the relaxation behavior of their lattices subjected to these symmetry-conserving strains through characteristic ratios of the elastic constants, which we determine from an explicit treatment of these strain cases. Furthermore, for the strained crystals we calculate the dielectric constants, the Born effective charges, and the zone-center phonon frequencies. The internal-strain effects are explicitly taken into account. The energies of the lowest conduction band and the highest valence bands are calculated to obtain the strain dependence of the interband transitions. The calculational methods are described in Sec. II, whereas the results are discussed in Sec. III. Finally, in Sec. IV a brief summary is given.

II. CALCULATIONAL METHODS

A. Numerical approach

The numerical computations are performed in the framework of the density-functional theory (DFT) within the local-density approximation (LDA). Explicitly, a pseudopotential-plane-wave code is used. Details of the method may be found in Refs. 19 and 20. The electron-electron interaction is described by the Perdew-Zunger interpolation.[21] The valence electron-ion interaction is treated by *ab initio* norm-

conserving pseudopotentials. They are generated according to the scheme of Troullier and Martins.[22] A nonlinear core correction (NLCC) is taken into account.[23] In this way we account for the effect of the semicore Ga $3d$ electrons. The electronic eigenfunctions are expanded into plane waves. The soft-core pseudopotentials allow the restriction to a relatively low cutoff energy of the plane-wave expansion. We use 75 Ry, i.e., a slightly larger value than in previous calculations of the unstrained nitrides.[19,20] This is a consequence of the high accuracy requirements for the determination of the atomic coordinates in the ground state considering differently strained crystals. The summation over the Brillouin zone (BZ) is performed using sets of Chadi-Cohen special points.[24] Convergence is reached for 12 points in the irreducible wedge of the BZ of the considered hexagonal crystal.

B. Strain and stress

The ground-state properties in the strain-free case are obtained by a minimization of the total energy with respect to the two lattice constants c and a as well as the dimensionless internal parameter u of the wurtzite structure. The equilibrium parameters $c_0=5.111$ (4.929) Å, $a_0=3.145$ (3.084) Å, and $u_0=0.3775$ (0.3825), resulting for unstrained GaN (AlN), are used to define the actual strain tensors. As perturbations we consider biaxial or uniaxial strain (or stress) with an orientation parallel to the c axis of the crystal. The accompanying deformations conserve the C_{6v}^4 space-group symmetry. Consequently, the strain tensor $\boldsymbol{\epsilon}$ is diagonal and possesses the components

$$\epsilon_{xx}=\epsilon_{yy}=(a-a_0)/a_0, \tag{1a}$$

$$\epsilon_{zz}=(c-c_0)/c_0. \tag{1b}$$

The internal strain is defined by the variation $(u-u_0)/u_0$. In the limit of small deviations from the equilibrium, Hooke's law gives the corresponding diagonal stress tensor $\boldsymbol{\sigma}$ with the elements

$$\sigma_{xx}=\sigma_{yy}=(C_{11}+C_{12})\epsilon_{xx}+C_{13}\epsilon_{zz}, \tag{2a}$$

$$\sigma_{zz}=2C_{13}\epsilon_{xx}+C_{33}\epsilon_{zz}. \tag{2b}$$

In Eqs. (2) four of the five independent stiffness constants C_{ij} of the considered wurtzite crystal occur. The modifications of Eqs. (2) by the built-in electric field due to the spontaneous and piezoelectric polarization are neglected because of their smallness.

In the general case of a uniaxial stress, the external forces vanish in the plane perpendicular to the stress direction and, hence, there is an elastic relaxation of the lattice in this plane. The ratio of the resulting in-plane strain to the deformation along the stress direction is expressed by the Poisson ratio, which in the general case can be anisotropic. For the wurtzite lattice subjected to a uniaxial stress σ_{zz} parallel to the c axis, $\sigma_{xx}=\sigma_{yy}=0$ holds. Then Eqs. (2) give the relation $\epsilon_{xx}=-\nu\epsilon_{zz}$, with the coefficient

$$\nu=\frac{C_{13}}{C_{11}+C_{12}}, \tag{3}$$

i.e., the Poisson ratio for this case. We refer to the accompanying deformation as uniaxial strain. To treat the uniaxial case we keep the lattice constant c fixed, and determine a and u by energy minimization. This is done for a set of values near c_0 and, in the linear limit, the coefficient ν follows immediately. By definition, the uniaxial stress is related to the strain along the direction of the stress by the Young modulus. In the case under consideration, this reads $\sigma_{zz}=E\epsilon_{zz}$, and the Young modulus is given by

$$E=C_{33}-\frac{2C_{13}^2}{C_{11}+C_{12}}. \tag{4}$$

A homogeneous biaxial stress in the plane perpendicular to the c axis of the wurtzite lattice is described by constant forces in this plane, $\sigma_{xx}=\sigma_{yy}$, and vanishing forces along the c axis, $\sigma_{zz}=0$. Then Hooke's law [Eqs. (2)] gives a relationship between the strain components, $\epsilon_{zz}=-R^B\epsilon_{xx}$, with the coefficient

$$R^B=\frac{2C_{13}}{C_{33}}. \tag{5}$$

Likewise, this deformation is also referred to as biaxial strain. In order to determine the biaxial relaxation coefficient R^B, we choose lattice constants a close to the equilibrium one and, in each case, minimize the total energy of the system with respect to the second lattice constant c and the internal parameter u to obtain the relaxed value of c. The in-plane stress is related to the in-plane strain by the biaxial modulus. This reads $\sigma_{xx}=Y\epsilon_{xx}$, and the biaxial modulus is given in terms of the elastic stiffness constants as

$$Y=C_{11}+C_{12}-\frac{2C_{13}^2}{C_{33}}. \tag{6}$$

In some cases, a relation to the strain along the c axis is useful, which obviously reads $\sigma_{xx}=-(Y/R^B)\epsilon_{zz}$. Since here the Young modulus is related to the biaxial modulus via

$$E=\frac{C_{33}Y}{C_{11}+C_{12}}=\frac{2\nu}{R^B}Y, \tag{7}$$

the former relation can also be expressed as

$$\sigma_{xx}=-\frac{1}{2\nu}E\epsilon_{zz}. \tag{8}$$

The last equation is also known to hold for elastically isotropic media.[25] Nevertheless, it is not restricted to that case, since here it also holds for the wurtzite symmetry due to the special strain case under consideration.

Finally, in the case of hydrostatic pressure p the (nonzero) components of the stress tensor are equal, $\sigma_{xx}=\sigma_{yy}=\sigma_{zz}=-p$, and from Hooke's law it follows that $\epsilon_{zz}=R^H\epsilon_{xx}$, with the ratio

$$R^H = \frac{C_{11}+C_{12}-2C_{13}}{C_{33}-C_{13}}. \tag{9}$$

However, in the explicit calculation of the elastic stiffness constants we consider the sum $(C_{11}+C_{12})$ as an independent quantity, and make use of the relation of the elastic constants to the isothermal bulk modulus:

$$B_0 = \frac{(C_{11}+C_{12})C_{33}-2C_{13}^2}{C_{11}+C_{12}+2C_{33}-4C_{13}}. \tag{10}$$

Equation (10) can be derived from Eqs. (2) and the (linearized) relation $-\Delta p/B_0 = \Delta V/V_0 = 2\epsilon_{xx}+\epsilon_{zz}$, with the pressure variation Δp (around $p=0$ GPa), the corresponding change in volume ΔV, and the equilibrium volume V_0. Values for the bulk modulus B_0 have been obtained[26] by fitting the Vinet equation of state[27] to the calculated volume dependence of the total energy. Explicitly, we use the relations

$$Y = \left[2+\frac{1}{2}\left(\frac{1}{\nu}-4\right)R^B\right]B_0 \tag{11}$$

and

$$C_{13} = Y/\left(\frac{1}{\nu}-R^B\right) \tag{12}$$

to obtain the absolute values of the elastic constants.

C. Dielectric and dynamical quantities

The dielectric properties, i.e., the dielectric constants and the dynamical charges, as well as the lattice-dynamical properties, i.e., the eigenfrequencies and eigenvectors of the lattice vibrations, are calculated in the framework of the density-functional perturbation theory (DFPT) (Ref. 28) for resulting ''equilibrium'' geometries c, a, and u at a given biaxial or uniaxial strain defined by a parameter $\epsilon_\perp (=\epsilon_{xx}=\epsilon_{yy})$ or $\epsilon_{||}$ $(=\epsilon_{zz})$, respectively. Here a generalization of the DFPT (Ref. 19) is used that takes into account the NLCC. The DFPT allows a direct calculation of the high-frequency dielectric tensor $\boldsymbol{\varepsilon}_\infty$ and the tensor of the Born effective charges, $\mathbf{Z}_B$. Their combination gives the nonanalytical contribution to the dynamical matrix due to long-range macroscopic electric fields. The tensor components of the static dielectric constant, $\boldsymbol{\varepsilon}_s$, are derived from a generalized Lyddane-Sachs-Teller relation[29]

$$(\varepsilon_s)_{\alpha\alpha}/(\varepsilon_\infty)_{\alpha\alpha} = \omega_{\mathrm{LO}}^2(\alpha)/\omega_{\mathrm{TO}}^2(\alpha). \tag{13}$$

A certain tensor component ($\alpha = x$ or z) is related to the zone-center LO- and TO-phonon frequencies of the wurtzite crystal belonging to the displacement direction α and, hence, to a certain symmetry E_1 or A_1. The differences of the corresponding frequency squares,

$$\omega_{\mathrm{LO}}^2(\alpha)-\omega_{\mathrm{TO}}^2(\alpha) = \frac{e^2(Z_B^*)_{\alpha\alpha}^2}{\varepsilon_0 V\mu}, \tag{14}$$

$$(Z_B^*)_{\alpha\alpha}^2 = (Z_B)_{\alpha\alpha}^2/(\varepsilon_\infty)_{\alpha\alpha}, \tag{15}$$

are directly related to the tensor components of the square of the ionic plasma frequency and, hence, to that of the screened Born effective charge, $(Z_B^*)_{\alpha\alpha}$, with the reduced mass μ of the cation-nitrogen pair, the effective volume V per pair, and the dielectric permittivity constant ε_0.[30]

In general, the resulting phonon frequencies of a strained wurtzite crystal are shifted or split with respect to the strain-free values. In the linear strain limit these shifts and splittings are related to the strain tensor $\boldsymbol{\epsilon}$ by[31–33]

$$\Delta\omega(A_1) = a(A_1)(\epsilon_{xx}+\epsilon_{yy})+b(A_1)\epsilon_{zz}, \tag{16a}$$

$$\Delta\omega(E_{1/2}) = a(E_{1/2})(\epsilon_{xx}+\epsilon_{yy})+b(E_{1,2})\epsilon_{zz} \pm c(E_{1/2})\sqrt{(\epsilon_{xx}-\epsilon_{yy})^2+4\epsilon_{xy}^2} \tag{16b}$$

in dependence on the mode symmetry $j=A_1$ or $E_{1/2}$. The non-Raman-active B_1 modes follow a similar relation as the A_1 modes. The coefficients $a(j)$, $b(j)$, and $c(j)$ are the corresponding phonon deformation potentials per unit strain. Since here we are considering symmetry-conserving strains, the tensor $\boldsymbol{\epsilon}$ is diagonal and only the deformation potentials $a(j)$ and $b(j)$ are involved.[34] They are determined directly from the *ab initio* calculations by the following ''artficial'' deformation. While keeping one lattice constant fixed at its equilibrium value, the other one is slightly strained, and the internal parameter u is determined from energy minimization. For this artificial strain state, the phonon frequencies are calculated, and the differences to the ground-state values immediately give the respective deformation potentials as linear coefficients.

For the considered cases of biaxial and uniaxial strain the diagonal elements of the strain tensor, ϵ_{xx} and ϵ_{zz}, are related to each other by the ratios R^B (biaxial case) or ν (uniaxial case). Consequently, one can relate the linear frequency shift directly to the given biaxial strain $\epsilon_\perp$ or uniaxial strain $\epsilon_{||}$. We write the shift as

$$\Delta\omega(j) = K_{\perp/||}(j)\epsilon_{\perp/||}. \tag{17}$$

The strain coefficients $K_{\perp/||}(j)$ are related to the deformation potentials by $K_\perp(j) = 2a(j)-R^B b(j)$ and $K_{||}(j) = -2\nu a(j)+b(j)$ for all zone-center phonon modes $j=A_1$(LO and TO), E_1(LO and TO), E_2(high and low), and B_1(high and low). However, we determine the values of the strain coefficients directly from the calculated phonon frequency shifts under biaxial and uniaxial strain. Furthermore, using the respective stress-strain relation, the frequency shifts (17) can be related to the corresponding uniaxial $\sigma_{||}$ or biaxial $\sigma_\perp$ stress parameter. Thereby, in the linear stress limit one obtains the coefficients $\tilde{K}_{\perp/||}(j)$ giving the frequency change per unit stress as $\tilde{K}_\perp(j) = K_\perp(j)/Y$ and $\tilde{K}_{||}(j) = K_{||}(j)/E$.

D. Electronic structure

In the wurtzite case of GaN and AlN the lowest conduction (c) band and the top of the valence (v) bands are situ-

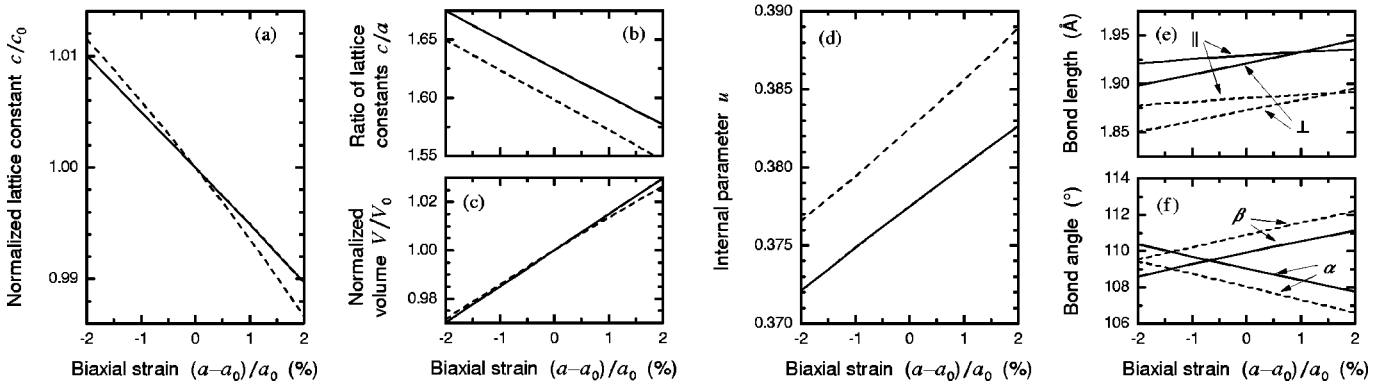

FIG. 1. Parameters of the atomic geometry vs the biaxial strain. GaN: solid line; AlN: dashed line. The lattice constant c (a), the ratio of lattice constants c/a (b), the normalized volume V/V_0 (c), the internal parameter u (d), the bond lengths (e), and the bond angles (f) are considered. The bonds along the c axis (nearly perpendicular to it) are labeled by $\|$ ($\perp$). The label α (β) denotes the angle between the bond parallel to the c axis and (one of) the three bonds nearly perpendicular to it (between two bonds nearly perpendicular to the c axis).

ated at the Γ point in the BZ. Without spin-orbit interaction they are related to an s-like Γ_{1c} state and to p-like Γ_{6v} and Γ_{1v} states. The two latter states are separated by a crystal-field splitting $\Delta_{\rm cr}=\varepsilon_{\Gamma_{6v}}-\varepsilon_{\Gamma_{1v}}$. Two energy gaps can be defined by $E_{A/B}=\varepsilon_{\Gamma_{1c}}-\varepsilon_{\Gamma_{6v}}$ and $E_C=\varepsilon_{\Gamma_{1c}}-\varepsilon_{\Gamma_{1v}}$, according to the optical transitions $\Gamma_{6v}\rightarrow\Gamma_{1c}$ (A,B) and $\Gamma_{1v}\rightarrow\Gamma_{1c}$ (C). In GaN, $E_{A/B}$ is the fundamental gap, whereas in AlN it is the C transition gap due to the negative crystal field splitting.[35,36] The applied strain influences both the energy gap and the crystal-field splitting. Without spin-orbit interaction the relevant energy levels are described by[6]

$$\varepsilon_{\Gamma_{1c}}(\boldsymbol{\epsilon})=\varepsilon_{\Gamma_{1c}}(0)+a_{cz}\epsilon_{zz}+a_{cx}(\epsilon_{xx}+\epsilon_{yy}), \tag{18a}$$

$$\varepsilon_{\Gamma_{6v}}(\boldsymbol{\epsilon})=\varepsilon_{\Gamma_{6v}}(0)+D_1\epsilon_{zz}+D_2(\epsilon_{xx}+\epsilon_{yy})+D_3\epsilon_{zz}+D_4(\epsilon_{xx}+\epsilon_{yy}), \tag{18b}$$

$$\varepsilon_{\Gamma_{1v}}(\boldsymbol{\epsilon})=\varepsilon_{\Gamma_{1v}}(0)+D_1\epsilon_{zz}+D_2(\epsilon_{xx}+\epsilon_{yy}). \tag{18c}$$

The electronic deformation potentials a_{cz}, a_{cx}, D_1, and D_2 characterize the effect of both hydrostatic and uniaxial strain contributions to the A/B energy gap. The deformation potentials D_3 and D_4 are related to the strain-induced changes of the crystal-field splitting. As a consequence the gap energies are given by[37]

$$E_{A/B}(\boldsymbol{\epsilon})=E_{A/B}(0)+a_1\epsilon_{zz}+a_2(\epsilon_{xx}+\epsilon_{yy})+b_1\epsilon_{zz}+b_2(\epsilon_{xx}+\epsilon_{yy}), \tag{19a}$$

$$E_C(\boldsymbol{\epsilon})=E_{A/B}(0)+\Delta_{\rm cr}(0)+a_1\epsilon_{zz}+a_2(\epsilon_{xx}+\epsilon_{yy}), \tag{19b}$$

with the deformation potentials $a_1=a_{cz}-D_1$ and $a_2=a_{cx}-D_2$ of the interband transitions. The quantities $b_1=-D_3$ and $b_2=-D_4$ are the deformation potentials of the crystal-field splitting. Its strain dependence is given as

$$\Delta_{\rm cr}(\boldsymbol{\epsilon})=\Delta_{\rm cr}(0)-b_1\epsilon_{zz}-b_2(\epsilon_{xx}+\epsilon_{yy}). \tag{20}$$

Analogously to the phonon deformation potentials, the electronic ones are also determined from the ''artificial'' strains mentioned above. Equations (19) also allow the definition of the strain coefficients $(\partial E_i/\partial\epsilon_j)|_{\boldsymbol{\epsilon}=\mathbf{0}}$ $(i=A,B,C$ and $j=\perp,\|)$ of the optical transition energies for the cases of biaxial and uniaxial strain, respectively. Again, these are determined directly from the corresponding strains. As for the phonon frequency shifts, using the respective stress-strain relation these strain coefficients can be directly converted to the corresponding coefficients $(\partial E_i/\partial\sigma_j)|_{\boldsymbol{\sigma}=\mathbf{0}}$ per unit stress.

III. RESULTS AND DISCUSSION

A. Strained structures

Structural results of the total-energy optimizations are presented in Figs. 1 and 2 for biaxial and uniaxial strain, respectively. As expected, due to the lattice relaxation (Poisson effect) one observes a decrease of the c (a) lattice constant with increasing tensile biaxial (uniaxial) strain. From these relations we immediately obtain the coefficients R^B and ν, which are listed and compared with other theoretical and experimental data (derived from the elastic stiffness constants) in Table I. In general, the behavior of GaN and AlN is rather similar. Although it is difficult to conclude for which material the respective relaxation effect is more pronounced, it can be noticed that the effect of biaxial strain (as expressed by the ratio R^B) is larger than that of uniaxial strain (as expressed by ν) by a factor of about 2.6 for GaN and 2.9 for AlN.

Correspondingly, for both materials the change in volume is much larger for biaxial than for uniaxial strain. The fractional volume change $\Delta V/V_0=2\epsilon_{xx}+\epsilon_{zz}$ amounts to $(2-R^B)\epsilon_\perp$ in the biaxial case and to $(1-2\nu)\epsilon_\|$ in the uniaxial one. The values of the prefactors are found exactly as the slope of the curves in Figs. 1(c) and 2(c). The internal parameter u and, hence, the internal strain $(u-u_0)/u_0$ obviously show a different strain behavior than the lattice constants, which is nevertheless systematic: It always changes in the opposite way to the ratio of the lattice constants. As c/a shrinks, u increases (and vice versa), regardless of the strain type (uniaxial or biaxial). The same behavior was also found under hydrostatic pressure.[26] It corresponds to the tendency of the wurtzite lattice to be resistant to changes of its bond

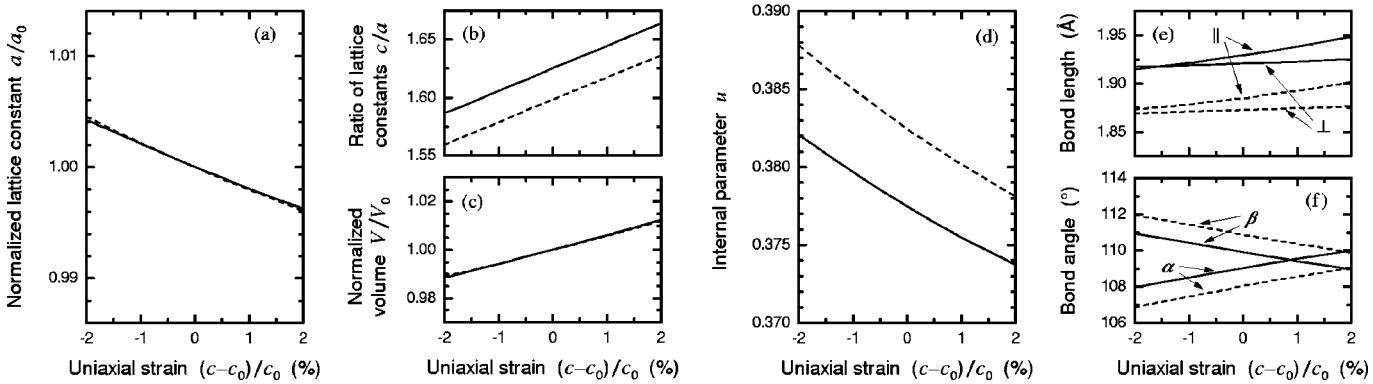

FIG. 2. Parameters of the atomic geometry vs the uniaxial strain. As in Fig. 1 but instead of c the lattice constant a is studied in (a).

lengths, as pointed out by Wright.[38] The linear strain coefficients are summarized in Table II. Again, they are not so very different for the two nitrides considered.

The rather strong internal strain effects dominate the variations of the bond lengths and bond angles [Figs. 1(e), 1(f), 2(e), and 2(f)]. Interestingly, the lengths $d_{||}=uc$ of the bonds parallel to the c axis increase in both strain cases. The effect is stronger for uniaxial strain. This follows the increase of c directly. Moreover, even in the case of biaxial strain the decrease of the c-lattice constant is accompanied by an increase of the bond lengths parallel to the c axis. The lengths $d_{\perp}=\sqrt{\frac{1}{3}a^2+(\frac{1}{2}-u)^2c^2}$ of the bonds nonparallel to the c axis also increase with tensile biaxial strain, while in the uniaxial case there is more or less a compensation of the variations of c, a, and u, resulting in almost constant bond lengths of that kind. For certain strain values, all bond lengths of one material become equal. However, this does not result in ideal tetrahedra, since the bond angles remain different.

The opposite behavior of the bond angles α and β versus biaxial or uniaxial strain is particularly interesting. There is a tendency for the reduction of the deformation of the bonding tetrahedra for compressive biaxial strain or tensile uniaxial strain. The angles approach the value 109.47° of the ideal tetrahedron. However, again, the tetrahedra remain deformed because of unequal bond lengths. In the opposite directions, tensile biaxial strain and compressive uniaxial strain, the bonding zigzag chains perpendicular to the c axis are flattened, i.e., the bonding tetrahedra are compressed along the c axis by shrinking the vertical distance $(\frac{1}{2}-u)c$ of the X-N layers ($X=$Ga,Al) toward a planar structure. The angle α tends toward 90°, whereas the angles β tend toward 120°. This implies a tendency for dehybridization from ideal sp^3 hybrids toward sp^2 and p_z orbitals.

B. Elastic behavior and stiffness constants

For cubic crystals and for elastically isotropic materials, $R^B=2\nu/(1-\nu)$ holds. Due to their uniaxial crystal structure, the wurtzite nitrides should exhibit an anisotropic behavior, and the comparison of the ratio $2\nu/(1-\nu)$ with the actual value of R^B provides information about the deviation of their elastic properties from cubic behavior. From Table I it is obvious that for GaN, $2\nu/(1-\nu)$ comes rather close to R^B, while for AlN there are significant differences. The deviating behavior of the two nitrides under consideration is also visible in the presence of hydrostatic pressure. From the R^H values of Table I it follows that, in this case, only GaN exhibits an approximately homogeneous dilatation (i.e., a proportional contraction) since $R^H_{\mathrm{GaN}}\approx 1.0$, while for AlN the compression is anisotropic ($R^H_{\mathrm{AlN}}\approx 1.2$). This was observed directly in high-pressure x-ray-diffraction experiments,[56,57] and was also found in *ab initio* calculations for hydrostatic pressure.[26,58,59] Therefore, the quality of calculations and measurements of elastic stiffness constants of wurtzite GaN and AlN can be easily characterized by the dimensionless quantities R^B, ν, $2\nu/(1-\nu)$, and R^H. For instance, in the case of GaN it appears that reliable values are close to $R^B=0.50\ldots 0.56$, $\nu=0.20\ldots 0.21$, $2\nu/(1-\nu)=0.49\ldots 0.54$, and $R^H\approx 1.0$. The situation is less clear for AlN, since the deviations between the results are larger. Nevertheless, the values can be expected to lie in the range $R^B=0.5\ldots 0.6$, $\nu=0.18\ldots 0.21$, $2\nu/(1-\nu)=0.45\ldots 0.53$, and $R^H\gtrsim 1.2$.

The reason for these differences between GaN and AlN can be traced back to the elastic stiffness constants, which are also listed in Table I. Our results are in excellent agreement with other *ab initio* calculations.[38] This holds in particular for AlN. In the case of GaN, the stiffness constants calculated within our method are slightly larger, mainly due to the relatively small value of R^B. The agreement with recently measured values[44–47] is reasonable for both nitrides. Therefore, since in our case all quantities arise from the same type of DFT calculations, the derived elastic constants represent a reliable basis for the extraction of phonon and electronic deformation potentials. There is also satisfying agreement with another recent calculation,[39] although the presented C_{33} value for GaN stands out. Nevertheless, considering the mentioned ratios of the stiffness constants R^B, R^H, and ν, the results of this calculation also provide a reasonable description of the elastic properties of the wurtzite nitrides. This also holds in part for those of the semi-*ab initio* calculation for AlN,[40] except for the too large $C_{11}+C_{12}$ and the somewhat larger moduli B_0, E, and Y. On the other hand, the calculated results of Ref. 41, which are obatined using the full-potential linear muffin-tin-orbital (FP-LMTO) method, show too large a $C_{11}+C_{12}$ for GaN (therefore, the

TABLE I. Elastic stiffness constants (in GPa) as well as related moduli and coefficients (see the text) compared with results of other (semi-) *ab initio* calculations[a–f] and measurements[g–s]. Underlined values for the bulk modulus are obtained directly from total-energy calculations, all other ones are derived from the elastic stiffness constants using Eq. (10). The experimental values from Refs. 50 and 51 are not directly measured but are derived from fits to other published data and, therefore, are given in parenthesis. The experimental values from Ref. 49 are recommended values ''based on the average of consistent measurements[g,i,j,r,s] '' and, therefore, are given in braces.

	R^B	ν	$\frac{2\nu}{1-\nu}$	R^H	Y	E	B_0	$C_{11}+C_{12}$	C_{13}	C_{33}
GaN										
present	0.502	0.202	0.506	0.99	463	373	<u>207</u>	515	104	414
calc.[a]	0.509	0.205	0.516	0.98	450	363	202	502	103	405
calc.[b]	0.553	0.212	0.538	1.04	432	332	197	490	104	376
calc.[d]	0.510	0.185	0.454	1.16	489	355	207	540	100	392
calc.[e]	0.269	0.119	0.269	1.00	523	461	201	540	64	476
exper.[g]	0.533	0.198	0.494	1.11	479	356	210	535	106	398
exper.[i]	0.564	0.212	0.538	1.07	458	343	208	520	110	390
exper.[j,k]	0.598	0.228	0.591	1.02	432	329	204	500	114	381
exper.[l]	{0.504}	{0.190}	{0.469}	{1.10}	{467}	{352}	{201}	{516}	{98}	{389}
exper.[n]	(0.593)	(0.222)	(0.570)	(1.06)	(376)	(281)	(175)	(433)	(96)	(324)
exper.[p]	1.18	0.371	1.18	1.01	239	150	195	426	158	267
exper.[q]	1.09	0.212	0.538	3.25	413	161	173	537	114	209
exper.[r]	0.416	0.156	0.370	1.15	481	362	192	514	80.4	387
exper.[s]	0.413	0.156	0.370	1.15	481	362	192	514	80.0	387
AlN										
present	0.611	0.210	0.532	1.21	469	322	<u>210</u>	538	113	370
calc.[a]	0.579	0.203	0.509	1.20	470	329	207	533	108	373
calc.[b]	0.585	0.207	0.522	1.17	474	337	212	540	112	383
calc.[c]	0.567	0.189	0.466	1.30	547	365	<u>240</u>	613	116	409
calc.[d]	0.665	0.236	0.618	1.11	454	322	218	538	127	382
calc.[f]	0.665	0.257	0.692	0.94	410	317	209	494	127	382
exper.[h]	0.509	0.177	0.430	1.25	510	354	210	560	99	389
exper.[i]	0.513	0.182	0.445	1.21	499	354	209	550	100	390
exper.[m]	(0.608)	(0.233)	(0.608)	(1.00)	(441)	(339)	(211)	(514)	(120)	(395)
exper.[n]	(0.714)	(0.235)	(0.614)	(1.25)	(496)	(326)	(237)	(596)	(140)	(392)
exper.[o]	0.608	0.255	0.685	0.84	397	334	201	470	120	395

[a]Reference 38.
[b]Reference 39.
[c]Reference 40.
[d]Reference 41.
[e]Reference 42, transformed from values for β-GaN.
[f]Reference 43.
[g]Reference 44.
[h]Reference 45.
[i]Reference 46.
[j]Reference 47.
[k]Reference 48, values for epitaxial layers.
[l]Reference 49.
[m]Reference 50.
[n]Reference 51.
[o]Reference 52.
[p]Reference 53.
[q]Reference 54.
[r]Reference 55.
[s]Reference 48, values for bulk samples.

corresponding R^H is also too large) and a slightly too large a C_{13} for AlN (so that R^B is somewhat too large and R^H somewhat too small). The FP-LMTO data that were transformed from zinc-blende GaN (Ref. 42) without taking into account lattice relaxation effects suffer from a too small C_{13}, which gives rise to a very small value of R^B. The low-cutoff-energy calculations of Ref. 43 for AlN, which accidentally give results similar to those of Ref. 41, result in too small a $C_{11}+C_{12}$, so that R^H is even smaller than 1.0. From the preceding discussion it follows that the latter results[41–43] should be used with caution.

Considering the experimental results, it can be noticed that although the elastic ratios are reasonable for the fitted values of Ref. 51 in the case of GaN, the moduli and stiffness constants are too small. The converse applies to AlN, where the moduli and stiffness constants of Ref. 51 compare well

TABLE II. Calculated strain-free values X_0 and linear strain coefficients $(1/X_0)(\partial X/\partial \epsilon_{\perp/||})_0$ of parameters of atomic geometry ($X=c,a,c/a,u,d_{||}$ and $d_\perp$); absolute lengths are in Å.

	GaN			AlN		
X	X_0	$\epsilon_\perp$	$\epsilon_{||}$	X_0	$\epsilon_\perp$	$\epsilon_{||}$
c	5.111	−0.502	1.000	4.929	−0.611	1.000
a	3.145	1.000	−0.202	3.084	1.000	−0.210
c/a	1.6252	−1.507	1.199	1.5982	−1.621	1.209
u	0.37747	0.694	−0.551	0.38245	0.805	−0.633
$d_{||}$	1.929	0.193	0.448	1.885	0.188	0.368
$d_\perp$	1.921	0.611	0.107	1.872	0.594	0.103

with the other data presented, except for the too large C_{13}. This causes the R^B and ν ratios likewise to be too large. The fitted values of Ref. 50 suffer from an underlying model for a cubic crystal, which is not justified for AlN. The measurements of Ref. 52 gave too low a value for $C_{11}+C_{12}$ of AlN, which results in $R^H<1.0$. For GaN, on the other hand, there are several measurements which show deviations for single elastic stiffness constants [too small a C_{13} (Refs. 48 and 55) and too small a C_{33} (Ref. 54)] which cause significant errors in the corresponding elastic ratios, but there is also one set of results the use of which should be completely avoided (Ref. 53). Unfortunately, this latter set of values has been published in the Landolt-Börnstein data collection.

According to Table I the relation $C_{11}+C_{12}\approx C_{13}+C_{33}$ holds with good accuracy for GaN but not for AlN. In agreement with the relations that are fulfilled for GaN, $R^H\approx 1.0$ and $2\nu/(1-\nu)\approx R^B$, the different elastic behavior of GaN and AlN is mainly determined by the larger $C_{11}+C_{12}$ value of AlN, which is also the reason for its larger biaxial modulus Y. The value of the ratio $R^B/[2\nu/(1-\nu)]=(C_{11}+C_{12}-C_{13})/C_{33}$ can serve as an estimate for a lower limit of R^H if it is larger than 1.0 (an upper limit if it is smaller than 1.0). Due to the quasicubic behavior, the relations between the elastic moduli for GaN can be approximated by simplified expressions. The biaxial modulus and the Young modulus are related to the bulk modulus via $Y\approx 3B_0(1-\frac{1}{2}R^B)=3B_0(1-2\nu)/(1-\nu)$ and $E\approx 3B_0(1-\frac{1}{2}R^B)/(1+\frac{1}{2}R^B)=3B_0(1-2\nu)$. These two moduli are related to each other by $E\approx Y/(1+\frac{1}{2}R^B)=Y(1-\nu)$. In each case, the conversion factors can be expressed using either the biaxial relaxation coefficient or the Poisson ratio, which themselves are in this case related to each other through $R^B=2\nu/(1-\nu)$, as mentioned above. Table I shows that these relations are by no means valid for AlN.

In contrast to the experimentally and theoretically well-established results for the hydrostatic coefficient R^H, there are contradictory reports on *direct* experimental results for the biaxial strain ratio R^B of GaN. No values are reported for AlN. The measured R^B_{GaN} values 0.689 (Ref. 60), 0.48 (Ref. 7), 0.45 (Ref. 2), 0.43 (Ref. 61), and 0.38 (Ref. 62; sometimes this value has been cited as the one for the Poisson ratio) show significant deviations among themselves. Additionally, from the results obtained in Ref. 63, a value of 0.386 can be extracted (which fits their data better than the one from the literature which they used), and from Fig. 1 of Ref. 64, a value of 0.45 can be obtained, if as strain-free reference for the lattice constants the data from Leszczynski *et al.*[65] are used. In addition, values of 0.457 (Ref. 66) as well as 0.400 and 0.384 (both from Ref. 67) have been calculated by *first-principles* methods. Except for the largest ones, these data significantly underestimate the results listed in Table I. The discrepancies become even more obvious if these values are used to derive elastic constants under the assumption of quasicubic behavior. The corresponding values for the Poisson ratio (except for $R^B=0.689$), according to the relation $\nu=R^B/(2+R^B)$, are obtained in the range 0.160–0.194. They again tend to be much smaller than those given in Table I. The elastic constants that can be derived from these data show the general trend that C_{13} comes out too small and all other values too large. Unfortunately, in the literature there are no reports on directly measured values of ν.

The reasons for these deviations are not clear, but some aspects may be mentioned. To determine the strain, a reference value has to be known which corresponds to a fully relaxed crystal and therefore represents the strain-free case. Generally, the lattice constants of GaN show unusually large fluctuations,[68] and it is difficult to determine the ''true'' unstrained values.[65] Here we mention that, strictly speaking, for the purpose of the investigation of elastic relaxation this reference value has to be understood as describing a crystal *free from external stress*. Internal stress effects due to defects, substituent atoms, and free carriers can still be present but need not be corrected for, since in principle it is the *same* crystal which is considered in both stressed and stress-free states. The biaxial relaxation behavior manifests itself in the slope of the c versus the a lattice constant, independent of their equilibrium values. It was shown that only if the biaxial relaxation coefficient R^B is extracted from the *measured slope*, the equilibrium value of c/a is of minor numerical influence.[2] Since the equilibrium is in each case defined by the condition $\boldsymbol{\sigma}=\mathbf{0}$, the corresponding lattice constants may vary between different samples. Therefore, ''the'' pair of reference values a_0, c_0 of an ideal GaN crystal may not be universally applicable. Nevertheless, usually such lattice constants are assumed to be independent of the doping level, the density of defects etc. Furthermore, the above-mentioned R^B_{GaN} values were obtained from a comparison of different samples, not from one single crystal that was subjected to varying stress or strain states (as in the case of hydrostatic

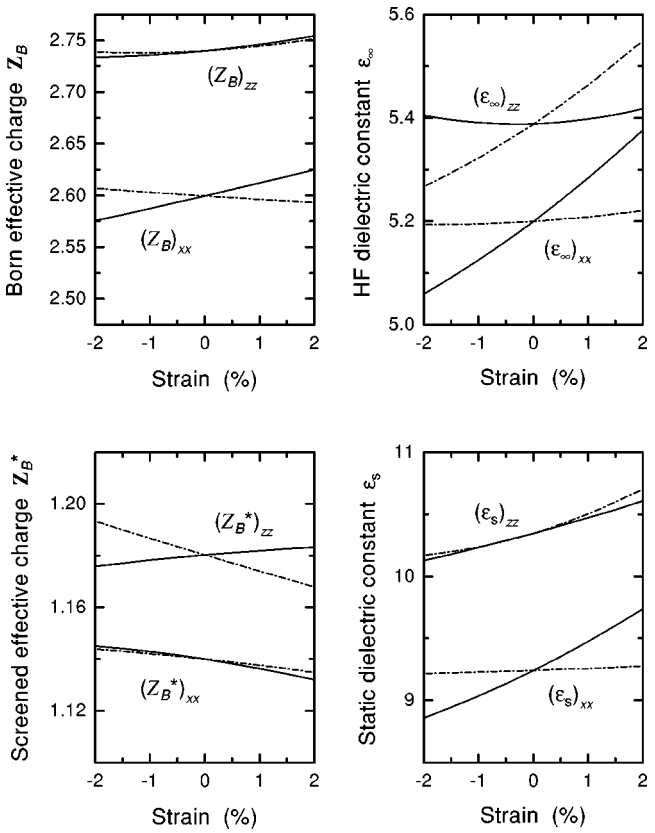

FIG. 3. Tensor components (xx, zz) of the Born (screened) effective charge $\mathbf{Z}_B$ ($\mathbf{Z}_B^*$) and the high-frequency (static) dielectric constant $\boldsymbol{\varepsilon}_\infty$ ($\boldsymbol{\varepsilon}_s$) of GaN vs strain. Solid line: biaxial strain $\boldsymbol{\epsilon}_\perp$; dot-dashed line: uniaxial strain $\boldsymbol{\epsilon}_{||}$.

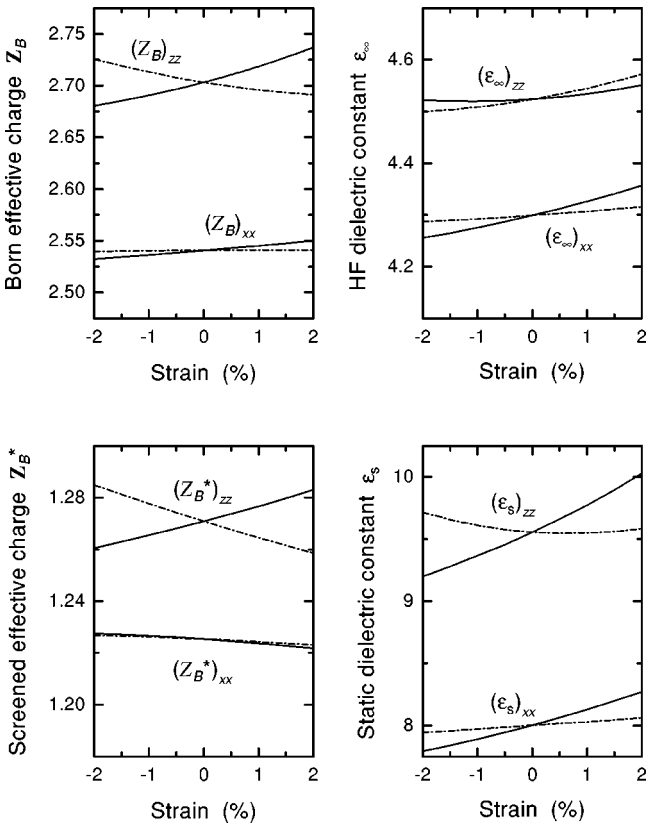

FIG. 4. As in Fig. 3, but for AlN.

pressure). In contrast, the elastic stiffness constants have been measured for only one sample and can therefore be expected to be more reliable in representing the elastic behavior of the wurtzite nitrides. To resolve this problem, combined x-ray and uniaxial-pressure experiments are called for in order to directly observe the Poisson effect of GaN and AlN single crystals.

C. Dynamic charge and dielectric constant

The Born and screened effective charges as well as the high-frequency and static dielectric constants behave rather similarly for GaN (Fig. 3) and AlN (Fig. 4), at least considering the sign of the linear strain coefficients for biaxial or uniaxial strain (Table III). The most significant exceptions concern the zz component of both the Born charge and the static dielectric constant versus uniaxial strain. There is a monotonic increase with strain for GaN, whereas a decrease is observed for AlN. For uniaxial strain, the xx component of the Born charge behaves in the opposite manner in GaN and AlN.

In the majority of cases, the quantities in Figs. 3 and 4 behave more or less differently versus biaxial and uniaxial strain. The main reason is the opposite effect of the strains parallel and perpendicular to the c axis. For GaN, the components of the high-frequency dielectric constant nearly follow the behavior of the corresponding bond lengths (parallel and nearly perpendicular to the c axis). The same trend holds for AlN, but is much less pronounced. The in-plane tensor components of the screened effective charges of both GaN and AlN are rather insensitive to both biaxial and uniaxial strain. On the other hand, the zz components show opposite trends with biaxial or uniaxial strain. For GaN, this is due to the opposite trends of $(\varepsilon_\infty)_{zz}$, whereas for AlN this originates from the behavior of $(Z_B)_{zz}$.

Apart from the in-plane components of the dielectric constants as functions of uniaxial strain, the other dielectric components in Figs. 3 and 4 (right panels) as well as in Table III (lower part) indicate remarkable changes induced by strain. Outstanding examples are the static dielectric constants and $(\varepsilon_\infty^{\mathrm{GaN}})_{xx}$ versus the biaxial strain. They possess the largest strain coefficients of all quantities considered. Apart from $(\varepsilon_s)_{zz}$ of AlN in the case of uniaxial distortions the strain coefficients in Table III are positive. However, some components exhibit a rather nonlinear behavior. This holds in particular for $(\varepsilon_\infty)_{zz}$ versus biaxial strain and $(\varepsilon_s)_{zz}$ versus uniaxial strain.

At vanishing strain, we calculate the values $(\varepsilon_\infty)_{xx}=5.20$ (4.30), $(\varepsilon_\infty)_{zz}=5.39$ (4.52), $(\varepsilon_s)_{xx}=9.24$ (8.00), and $(\varepsilon_s)_{zz}=10.35$ (9.56) for GaN (AlN), in close agreement with experimental data. Available experimental values are $(\varepsilon_s^{\mathrm{GaN}})_{xx}=9.5$,[69] 9.28 (Ref. 70) and $(\varepsilon_s^{\mathrm{GaN}})_{zz}=10.4$,[69] 10.2,[70] $(\varepsilon_s^{\mathrm{AlN}})_{xx}=7.98$,[71] 8.3 (Ref. 72) and $(\varepsilon_s^{\mathrm{AlN}})_{zz}=9.18$,[71] 8.9 (Ref. 72) as well as $\varepsilon_s^{\mathrm{AlN}}=8.50$ (determined from a polycrystalline sample)[73]; furthermore $(\varepsilon_\infty^{\mathrm{GaN}})_{xx}=5.35$,[69] 5.29,[70] 5.14 (Ref. 74) and $(\varepsilon_\infty^{\mathrm{GaN}})_{zz}=5.31$,[74] as well as $(\varepsilon_\infty^{\mathrm{AlN}})_{xx}=4.68$,[73]

TABLE III. Calculated strain-free values X_0 as well as linear and quadratic strain coefficients $(1/X_0)\times(\partial X/\partial\epsilon_{\perp/\|})_0$, $(1/X_0)(\partial^2 X/\partial\epsilon^2_{\perp/\|})_0$ of tensor components of dielectric properties ($X=\mathbf{Z}_B$, $\mathbf{Z}_B^*$, $\boldsymbol{\varepsilon}_\infty$, $\boldsymbol{\varepsilon}_s$, $\Delta\boldsymbol{\varepsilon}$). First value: linear coefficient; second value: quadratic coefficient.

	GaN					AlN				
X	X_0	$\epsilon_\perp$		$\epsilon_{\|\|}$		X_0	$\epsilon_\perp$		$\epsilon_{\|\|}$	
$(Z_B)_{xx}$	2.60	0.474	0.011	−0.133	0.006	2.54	0.175	0.010	0.011	−0.005
$(Z_B)_{zz}$	2.74	0.189	0.076	0.125	0.096	2.70	0.521	0.106	−0.319	0.098
$(Z_B^*)_{xx}$	1.14	−0.287	−0.065	−0.198	−0.027	1.23	−0.119	−0.028	−0.073	−0.017
$(Z_B^*)_{zz}$	1.18	0.157	−0.031	−0.536	0.016	1.27	0.441	0.036	−0.519	0.034
$(\varepsilon_\infty)_{xx}$	5.20	1.525	0.176	0.129	0.068	4.30	0.588	0.081	0.170	0.025
$(\varepsilon_\infty)_{zz}$	5.39	0.062	0.214	1.309	0.184	4.52	0.160	0.140	0.399	0.134
$(\varepsilon_s)_{xx}$	9.24	2.371	0.308	0.161	0.031	8.00	1.493	0.194	0.363	0.007
$(\varepsilon_s)_{zz}$	10.35	1.158	0.093	1.287	0.432	9.56	2.159	0.308	−0.339	0.489
$(\Delta\varepsilon)_{xx}$	4.04	3.460	0.240	0.201	−0.008	3.70	2.544	0.162	0.588	−0.007
$(\Delta\varepsilon)_{zz}$	4.96	2.347	−0.019	1.262	0.351	5.04	3.956	0.229	−1.002	0.404

4.64,[75] 4.4 (Ref. 72) and $(\varepsilon_\infty^{\mathrm{AlN}})_{zz}=4.8$.[72] This agreement allows a reliable discussion of the lattice contributions to the static polarizabilities of the group-III nitrides:

$$(\Delta\varepsilon)_{\alpha\alpha}=(\varepsilon_s)_{\alpha\alpha}-(\varepsilon_\infty)_{\alpha\alpha}=\frac{e^2(Z_B)^2_{\alpha\alpha}}{\varepsilon_0 V\mu\omega^2_{\mathrm{TO}}(\alpha)}. \qquad (21)$$

This expression follows from a combination of relations (13), (14), and (15). For nitrides the relative contribution of the lattice to ε_s is unusually large (approximately 50%), being about 1.5 times stronger than for SiC. Furthermore, the difference between the xx and zz components is strongly enhanced for the static constant compared to the HF dielectric constant, i.e., the anisotropy is much larger for ε_s than for ε_∞. This is due to the different LO-TO splittings for the A_1 and the E_1 phonon modes (see Sec. III D). The variation of the lattice polarizability for both directions $\alpha=x$ and z is relatively weak for uniaxial strain (cf. Table III). However, the linear coefficients for biaxial strain approach relatively large values as do already the coefficients of the dielectric constants themselves. That implies a remarkable increase of the lattice polarizability with rising values of tensile biaxial strain.

D. Zone-center phonon frequencies

The strain dependence of the Raman frequencies of modes with A_1, E_1, and E_2 symmetry as well as of the non-Raman active B_1 modes is plotted in Figs. 5 (GaN) and 6 (AlN). The A_1(LO) and E_1(TO) modes appear for phonon propagation parallel to the c axis, whereas E_1(LO), A_1(TO), and E_1(TO) are observable for propagation directions perpendicular to the c axis. The nonpolar B_1 and E_2 modes do not depend on the phonon propagation direction. There is a general tendency in the strain dependence for all modes under consideration except from the lower E_2 modes. With rising compressive strain the mode frequencies increase. This effect has already been observed for hydrostatic pressure.[26] However, it also occurs for biaxial and uniaxial distortions, but with different strengths. In general, the strain variations are larger in the biaxial case compared to the uniaxial one. However, the A_1(TO) and B_1^{low} modes in AlN remain nearly unaffected by uniaxial strain. Closer inspection reveals that they even show a weakly nonlinear behavior.

In the hydrostatic limit the effect can be explained by a general shortening of the bonds and, as a consequence

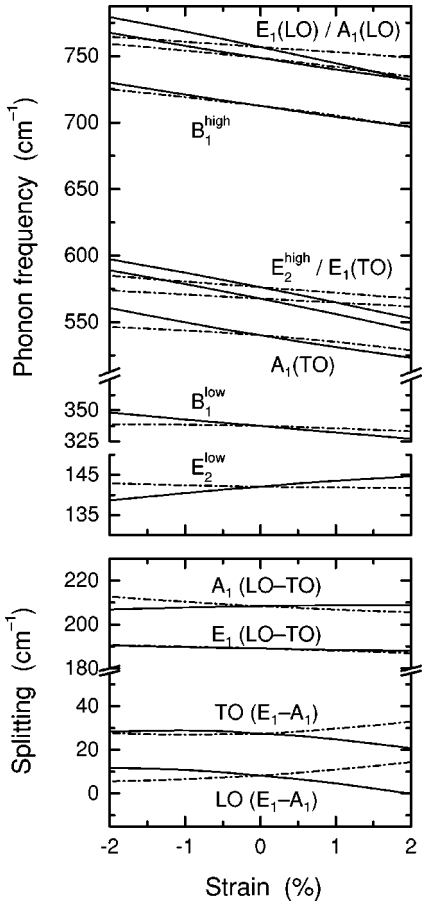

FIG. 5. Zone-center phonon frequencies of GaN vs biaxial strain $\epsilon_\perp$ (solid line) and uniaxial strain $\epsilon_{\|}$ (dot-dashed line). In addition, the LO-TO and anisotropy-related splittings are given.

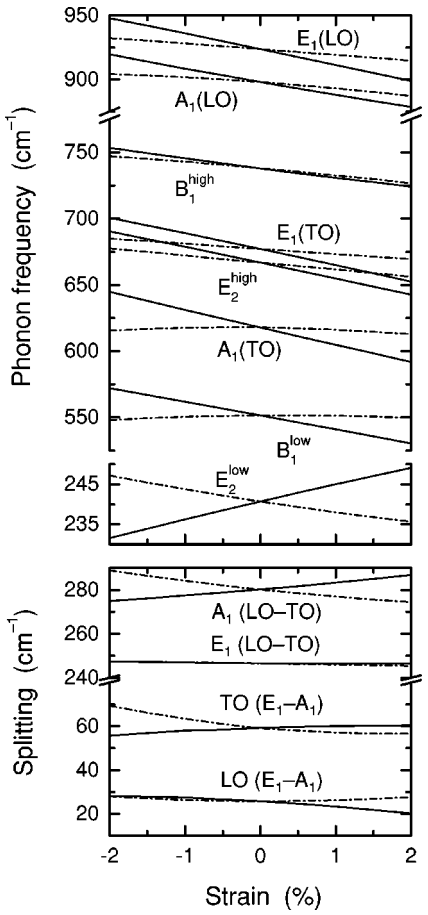

FIG. 6. As in Fig. 5, but for AlN.

thereof, an enlargement of the force constants. In the case of biaxial strain, i.e., a reduction of the *a*-lattice constant accompanied by a smaller increase of the *c*-lattice constant, this bond contraction occurs mainly for the three bonds nonparallel to the *c* axis (cf. Fig. 1). Similarly, under compressive uniaxial strain the bonds are also shortened, but in particular the one parallel to the *c* axis (cf. Fig. 2). However, the change in unit-cell volume that occurs along with these bond-length variations is much larger in the case of biaxial strain than for the uniaxial one, which partly accounts for the different magnitude of the frequency shifts.

The lower E_2 modes in Figs. 5 and 6 behave oppositely under biaxial and uniaxial strain. As under hydrostatic pressure, these modes are softened with rising compressive biaxial strain. However, in the presence of uniaxial strain the behavior of the lower E_2 modes is normal. The anomalous variation of the lower E_2 frequencies with biaxial strain is a consequence of the interplay of several elastic and Coulomb contributions to the lattice vibrations in the case of the lower E_2 mode.[77] For GaN, the experimentally determined phonon deformation potentials[7] confirm the positive sign of the biaxial mode coefficient, i.e., the mode softening. Recently, the shift of this mode to higher energy under tensile biaxial strain was also observed experimentally for AlN.[15]

The qualitatively similar effects of hydrostatic, biaxial, and uniaxial deformations on the zone-center phonon frequencies and the general shortenings of the bond lengths

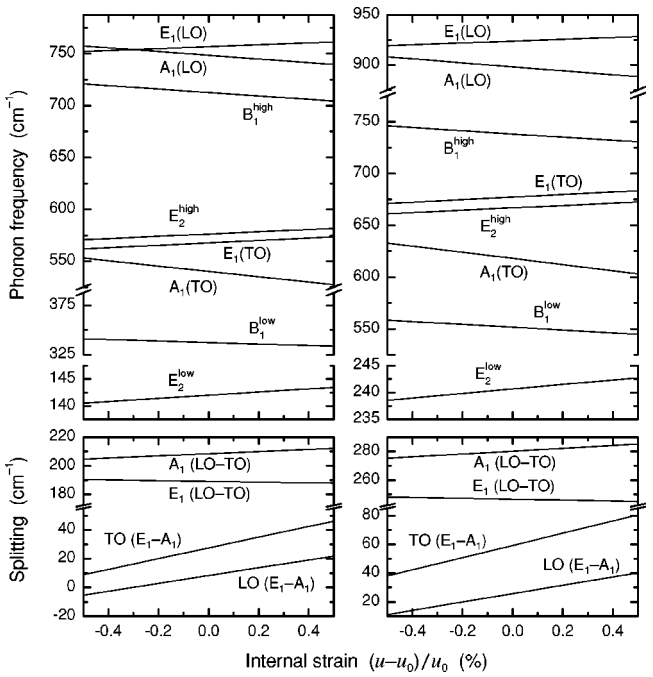

FIG. 7. Zone-center phonon frequencies and their splittings vs internal strain $(u-u_0)/u_0$. Left panels: GaN; right panels: AlN.

raise a question concerning the role of the internal strain. According to Figs. 1 and 2 the internal parameter *u* exhibits opposite behaviors for biaxial and uniaxial strain. For phonons, Fig. 7 indicates a clear symmetry dependence of the internal strain influence. Only the A_1 and B_1 modes follow the general behavior discussed for Figs. 5 and 6. Conversely, the E_1 and E_2 modes decrease their frequencies with increasing compressive internal strain. This is related to the fact that the A_1 and B_1 modes are accompanied by atomic displacements parallel to the *c* axis, whereas the corresponding E_1 and E_2 displacements point in the perpendicular direction. Therefore, the bond expansion parallel to the *c* axis and the corresponding contraction of the other bonds have different consequences.

The internal-strain dependences of the splittings of the polar optical phonon frequencies exhibit the opposite behavior. Whereas for the modes of E_1 symmetry the LO-TO splitting remains practically uninfluenced or decreases, in the A_1 case this splitting increases with increasing tensile internal strain. Additionally, from our computations we obtain that the screened effective charges hardly vary with the internal strain. Therefore, since the volume is fixed, according to expression (14) the changes of the splitting are mainly related to the opposite tendencies of the corresponding sum of frequencies. The increase of the splittings between the TO modes of different symmetry with increasing tensile internal strain (cf. Fig. 7) directly shows the increase of the elastic anisotropy in a unit cell. The anisotropy due to the macroscopic, long-range electric field is of opposite effect compared to the elastic one, because the E_1-A_1 splitting is reduced for the LO modes compared to that for the TO modes. Since the anisotropy of the macroscopic electric field depends only on the screened effective charges, it remains practically unchanged. The slightly smaller slope of the dif-

TABLE IV. Linear coefficients per unit strain, $K_{\perp/\|}(j)$ (in cm^{-1}), or per unit stress, $\tilde{K}_{\perp,\|}(j)$ (in $\mathrm{cm}^{-1}/\mathrm{GPa}$), of the zone-center vibrational modes j. The last two columns give values for the LO-TO splittings. The obtained biaxial coefficients are compared with experimental results (Refs. 7, 11–17, and 76). In some measurements the biaxial strain coefficient was obtained relative to the c-axis strain ϵ_{zz} and not to the in-plane strain $\epsilon_{\perp}$. For clarity, here we list the originally measured data and indicate the necessary conversion by the additional factor R^B. Where appropriate, the experimental coefficients are recalculated to correct for a wrong conversion formula or deviating values of the elastic stiffness constants. The resulting numbers are given in parentheses. The values in braces are obtained from a fit that covers a wider strain range.[e]

	E_2^{low}	B_1^{low}	A_1(TO)	E_1(TO)	E_2^{high}	B_1^{high}	A_1(LO)	E_1(LO)	LO–TO	
									A_1	E_1
GaN										
$K_{\perp}(j)$	154	−527	−931	−1139	−1115	−836	−885	−1198	46	−59
	268[a]		−641[a]	−1314[a]	−1258,[a]		−191 (−842)[b]			
					−693 (−1214),[b]					
					$-2632R^B$ (−1395),[c]					
					$-2537R^B$ (−1345)[d]					
$K_{\|\|}(j)$	−24	−149	−443	−300	−418	−696	−618	−389	−175	−89
$\tilde{K}_{\perp}(j)$	0.33	−1.14	−2.01	−2.46	−2.41	−1.81	−1.91	−2.59	0.10	−0.13
	0.5[a]		−1.4,[a]	−2.8[a]	−2.7[a],		−0.8 (−1.8)[b]			
			−3.0 {−2.1}[e]		−3.9 {−3.3}, [e]					
					−2.9 (−2.5),[b]					
					−4.2 (−2.9),[c]					
					−4.8 (−2.8),[d]					
					−2.4[f]					
$\tilde{K}_{\|\|}(j)$	−0.06	−40	−1.19	−0.80	−1.12	−1.87	−1.67	−1.04	−0.47	−0.24
AlN										
$K_{\perp}(j)$	439	−1047	−1330	−1208	−1198	−738	−1038	−1233	292	−25
					$-4398R^B$ (−2239),[g]					
					−1829[h]					
$K_{\|\|}(j)$	−288	40	−70	−391	−532	−516	−434	−442	−355	−51
$\tilde{K}_{\perp}(j)$	0.94	−2.23	−2.84	−2.58	−2.55	−1.57	−2.21	−2.63	0.62	−0.05
					−6.3 (−4.4),[g]					
					−3.9[h]					
$\tilde{K}_{\|\|}(j)$	−0.89	0.12	−0.22	−1.21	−1.65	−1.60	−1.35	−1.37	−1.10	−0.16

[a]Reference 7.
[b]Reference 11.
[c]Reference 12.
[d]Reference 13.
[e]References 16 and 76.
[f]Reference 14.
[g]Reference 15.
[h]Reference 17.

ference of the LO frequencies is due to the increasing A_1 (LO-TO) splitting and, therefore, results from the overall decrease of the frequencies of the modes with A_1 symmetry, as discussed above.

E. Phonon mode coefficients and deformation potentials

The linear strain coefficients $K_{\perp/\|}(j)$ (in cm^{-1}) are listed in Table IV. In addition, in this table the linear stress coefficients $\tilde{K}_{\perp/\|}(j)$ per unit stress (i.e., in units of $\mathrm{cm}^{-1}/\mathrm{GPa}$) are given. They are obtained from the strain coefficients $K_{\perp/\|}(j)$ using the calculated elastic stiffness constants presented in Table I. For GaN, these coefficients are compared with experimental results for $j=E_2^{\mathrm{low}}$, A_1(TO), E_1(TO), E_2^{high}, and A_1(LO).[7,11–14,76] For AlN, there are two experimental results for the E_2^{high} mode[15,17] only. For GaN, several experimental deformation potentials and stress coefficients exist for this mode. In general, good agreement is obtained with the coefficients measured by Davydov *et al.*[7] This holds not only for E_2^{high} but also for other modes, in particular for E_1(TO). The discrepancy concerning the A_1(TO) mode will be discussed below. For the stress coefficient of this mode, another experimental result[76] shows very good agreement when a larger set of samples is used for fitting, which then covers a wider strain range. The general trend that the calculated values tend to be somewhat smaller than the experimental ones is consistent with the same trend which was previously observed for the calculated hydrostatic pressure coefficients of the phonon modes,[77] $\tilde{K}^H(j)=[\partial\omega(j)/\partial p]_{p=0}$. Since the three

independently calculated coefficients fulfill the relation $\tilde{K}_\perp(j)+\tilde{K}_{||}(j)=-\tilde{K}^H(j)$, the stress coefficients can be expected to be likewise smaller (approximately 20%). It is not clear whether this is a shortcoming of the calculation or due to uncertainties in the experimental procedure.

It is important to notice that the originally published experimental biaxial mode coefficients only seldom are the directly measured data. Either the published values are already converted to stress coefficients via elastic stiffness constants,[12,14,15,76] or the mode coefficients have to be reconstructed from phonon deformation potentials[17] which have been obtained by means of additional mode pressure coefficients (or Grüneisen parameters), or both conversions have been made.[7,11] Due to these varying procedures, additional errors are introduced to the results. On the other hand, in Ref. 13 no such conversions were employed, and the strain coefficient was given only with respect to ϵ_{zz}, since the variation of the lattice constant c is measured. For this result, a correction is necesssary due to another source of error that occasionally occurs in the published values for $\tilde{K}_\perp$, which consists of the use of a wrong relation[78] between $\sigma_\perp$ and ϵ_{zz}. Furthermore, in Ref. 12 isotropic elastic moduli were unnecessarily extracted from the stiffness constants according to the Voigt average,[79] which applies only for polycrystalline samples that consist of crystallites having an arbitrary orientation. Therefore, we stress that the published values in several cases depend both on the parameter sets and the procedure used for their extraction from the ''raw'' experimental data. For instance, as the sets of experimental results for the elastic constants from Ref. 51 (cf. Table I) stand out both with respect to the absolute values for elastic constants of GaN (partially also for AlN) and with respect to the elastic relaxation coefficients of AlN, their use for the evaluation of stress-strain factors should be avoided, although, incidentally, Y has a reasonable value. Instead, if one employs the results of McNeil *et al.* (Ref. 45) for the elastic constants, the value of the mode coefficient for the high-frequency E_2 mode of AlN is considerably lowered.[15] Still, the agreement between experimental and theoretical results is not complete. Also, the result which can be extracted from the phonon deformation potentials of AlN given in Ref. 17 is considerably larger than the calculated one. Unfortunately, in the latter paper no details about the derivation procedure of the phonon deformation potentials were given.

In several papers the measured frequency shift versus the c-axis strain, $\Delta\omega/\epsilon_{zz}$, was given explicitly. Therefore, to minimize the influence of additional errors we prefer to list these original data in Table IV where possible. They are identified by the necessary conversion factor R^B, which has been added for consistency. In order to avoid the influence of the use of different formulas and elastic constants, we have partly recalculated the stress coefficients from the originally measured data. To be consistent, measured elastic stiffness constants have been used for both GaN (Ref. 44) and AlN.[45] The reevaluation brings the experimental results rather close to the calculated ones. This holds especially for the biaxial strain coefficients and the accompanying stress coefficients for the E_2^{high} and $A_1(\text{LO})$ modes of GaN. For these modes the agreement can be considered to be very good, taking into account the above-mentioned overall deviations. In general, comparing the calculated and measured coefficients for GaN and considering the uncertainties of the experimental results and the variations among the different measurements, the agreement between theory and experiment in Table IV is satisfactory. The considerable lowering of the value of the stress coefficient of the E_2^{high} mode of GaN due to the recalculation implies that, by using the Raman shift of this mode as a measure of the biaxial strain, up to now the accompanying stress has been underestimated.

Sometimes, in the case of a biaxially strained crystal a relation of the frequency shift to the relative volume change, $\Delta\omega(j)=-\omega_0(j)\gamma(j)\Delta V/V_0$, is used as an approximation, with the phonon frequency in a strain-free situation $\omega_0(j)$ and the mode Grüneisen parameter $\gamma(j)$. This relation is strictly valid only in the presence of hydrostatic pressure and, therefore, its application to the case of biaxial strain has to be justified. This simply means the use of $K'_\perp(j)=-\omega_0(j)\gamma(j)(2-R^B)$ instead of $K_\perp(j)=2a(j)-R^Bb(j)$. Since in terms of the phonon deformation potentials one has $K'_\perp(j)=[2a(j)+R^Hb(j)](2-R^B)/(2+R^H)$, in general, this ''hydrostatic approximation'' is only valid for those modes where the deformation potentials $a(j)$ and $b(j)$ are (nearly) equal. The calculated phonon frequency in the strain-free case and the deformation potentials are listed in Table V. The latter agree completely with the ones determined previously,[34] which were derived from the strain coefficients. Table V shows that for GaN the criterion of nearly equal values for $a(j)$ and $b(j)$ is fulfilled only for the E_2^{high}, holds approximately for the $A_1(\text{TO})$ and $E_1(\text{LO})$, but fails for the E_2^{low}, $E_1(\text{TO})$, and $A_1(\text{LO})$ modes. From the experimentally determined mode Grüneisen parameter[77] $\gamma(E_2^{\text{high}})=1.50$, the measured zero-pressure frequency[77] $\omega_0(E_2^{\text{high}})=567.0\ \text{cm}^{-1}$, and the elastic constants of Polian *et al.*[44] a numerical value of $K'_\perp(E_2^{\text{high}})=-1248\ \text{cm}^{-1}$ is obtained. Again using the elastic constants from Ref. 44, this corresponds to a value of the stress coefficient of $-2.6\ \text{cm}^{-1}/\text{GPa}$, which indeed approaches the calculated value given in Table IV. Previously, by using this approximation, a value of $-3024\ \text{cm}^{-1}R^B$ was obtained for the biaxial strain coefficient of this mode.[80] This is probably due to a mode Grüneisen parameter which is too large, since it was derived using a bulk modulus of 245 GPa.[81]

A more general interpretation of the strain effects on the phonon frequencies is possible in all cases of symmetry-conserving strains. With respect to the in-plane strain component, the strain tensor can be expressed as $\boldsymbol{\epsilon}=\epsilon_{xx}\ \text{diag}(1,1,R)$, where R can take any required value. For the special cases of hydrostatic pressure, biaxial strain, and uniaxial strain, it equals R^H, $-R^B$, and $-1/\nu$, respectively. Any strain of this type can be decomposed into an isotropic (accounting for the volume change) and a pure shear component (without change of the volume), $\boldsymbol{\epsilon}=\boldsymbol{\epsilon}^{\text{iso}}+\boldsymbol{\epsilon}^{\text{sh}}$, with $\boldsymbol{\epsilon}=\epsilon^{\text{iso}}\ \text{diag}(1,1,1)+\epsilon^{\text{sh}}\ \text{diag}(1,1,-2)$. The relative volume change is given by $\Delta V/V_0=3\epsilon^{\text{iso}}$. Since the trace of the

TABLE V. Phonon deformation potentials $a(j)$ and $b(j)$ (in cm^{-1}) for GaN and AlN. Additionally, the resulting isotropic and shear deformation potentials, $K^{iso}(j)=2a(j)+b(j)$ and $K^{sh}(j)=2[a(j)-b(j)]$, are given. The mode frequencies $\omega(j)$ (in cm^{-1}) calculated in the strain-free case are also listed.

	E_2^{low}	B_1^{low}	A_1(TO)	E_1(TO)	E_2^{high}	B_1^{high}	A_1(LO)	E_1(LO)
GaN								
$\omega(j)$	142	337	540	568	576	713	748	757
$a(j)$	75	−334	−640	−717	−742	−661	−664	−775
$b(j)$	4	−275	−695	−591	−715	−941	−881	−703
$K^{iso}(j)$	154	−943	−1975	−2025	−2199	−2263	−2209	−2253
$K^{sh}(j)$	142	−118	110	−252	−54	560	434	−144
AlN								
$\omega(j)$	241	552	618	677	667	738	898	924
$a(j)$	149	−580	−776	−835	−881	−601	−739	−867
$b(j)$	−223	−197	−394	−744	−906	−757	−737	−808
$K^{iso}(j)$	75	−1357	−1946	−2414	−2668	−1959	−2215	−2542
$K^{sh}(j)$	744	−766	−764	−182	50	312	−4	−118

shear deformation matrix vanishes, the decomposition is unique only up to an arbitrary factor that determines the magnitude of the shear deformation parameter, ϵ^{sh}. For the decomposition chosen here, the isotropic and the shear deformation parameter are given by $\epsilon^{iso}=\epsilon_{xx}(2+R)/3$ and $\epsilon^{sh}=\epsilon_{xx}(1-R)/3$. Correspondingly, any linear phonon frequency shift can be expressed as $\Delta\omega=(\Delta\omega)^{iso}+(\Delta\omega)^{sh}$, with $(\Delta\omega)^{iso}=(2a+b)\epsilon^{iso}$ and $(\Delta\omega)^{sh}=2(a-b)\epsilon^{sh}$. The corresponding phonon deformation potentials for the isotropic and shear deformation are therefore $K^{iso}(j)=2a(j)+b(j)$ and $K^{sh}(j)=2[a(j)-b(j)]$. They are given in Table V. Due to the mentioned indeterminateness of the value of the shear deformation parameter, the value of the shear deformation potential of the phonon frequency, K^{sh}, is unique only up to a common factor.

Whereas the isotropic deformation potentials are rather similar for GaN and AlN and, except for the E_2^{low} and B_1^{low} modes, take values of similar magnitude, the shear deformation potentials show significant differences, both between GaN and AlN and among their modes. A systematic trend is hard to find. For both materials, the shear deformation potential of the E_2^{high} mode is rather small, whereas that of the B_1^{high} mode is rather large. For both E_1 modes one has similar values for K^{sh} in GaN and AlN, with that of the LO mode being smaller than that of the TO mode. On the other hand, some modes show the opposite behavior in GaN and AlN: $K^{sh}[A_1(LO)]$ is small in AlN but large in GaN, and the opposite holds for the A_1(TO) mode. Finally, the K^{sh} values of the E_2^{low} and the B_1^{low} mode are very large in AlN but below average in GaN.

The three symmetry-conserving strains under consideration are completely different concerning their decomposition into isotropic and shear strain components. For both nitrides $\epsilon^{iso}/\epsilon_{xx}=-1(\frac{1}{2})$ and $\epsilon^{sh}/\epsilon_{xx}=2(\frac{1}{2})$ nearly hold in the case of uniaxial (biaxial) strain; furthermore $\epsilon^{iso}/\epsilon_{xx}=1$ in the case of hydrostatic pressure. However, in this case, the value of $\epsilon^{sh}/\epsilon_{xx}$ nearly vanishes for GaN but amounts to -0.07 for AlN. Therefore, in the hydrostatic pressure case the ratio $\epsilon^{sh}/\epsilon^{iso}$ is negligible only for GaN. This allows for an interpretation of unusual strain behaviors of some of the phonon modes. First, we come back to the lower E_2 modes. In AlN, the frequency of this mode shows a vanishing dependence on the hydrostatic pressure[77] but a significant variation with uniaxial and biaxial strain. The opposite behavior is found in GaN, where the uniaxial and biaxial strain dependences are rather weak, but in the case of hydrostatic pressure a distinct mode softening occurs. This stems from the fact that, for GaN, due to the nearly vanishing shear deformation under hydrostatic pressure, $\epsilon^{sh}/\epsilon_{xx}=0.003$, only the isotropic deformation potential is involved, whereas for AlN, due to the larger contribution of shear strain, there is a near cancellation of the influence of the isotropic and the shear deformation potential. The latter two potentials are of extremely different magnitudes in AlN, so that the frequency shifts of this mode under uniaxial and biaxial strain are dominated by the large shear deformation potential. In GaN, on the other hand, the isotropic and shear deformation potentials are nearly equal, and there is a partial compensation of their influence in the case of uniaxial strain and, due to their smallness, only a weak effect for biaxial strain. Second, we consider the B_1^{low} and A_1(TO) modes of AlN, which remain nearly unaffected by uniaxial strain. This behavior can be understood as a consequence of the very large shear deformation potential of these modes which nearly cancels the influence of the isotropic deformation potential, since for uniaxial strain the shear potential ''counts twice.'' This cancellation is almost complete for the B_1^{low} mode, which therefore shows a nearly vanishing strain dependence, and remains incomplete for the A_1(TO) mode, where a very weak strain dependence results.

F. Electronic energies

The influence of both biaxial and uniaxial strain is also investigated for the highest occupied electronic energy levels Γ_{6v} and Γ_{1v} and the lowest unoccupied level Γ_{1c}. The resulting energy gaps E_i of the $i=A,B$, and C optical transi-

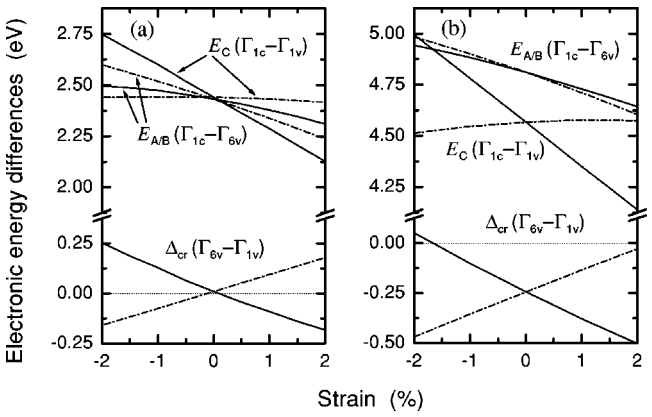

FIG. 8. Differences of electronic energy levels at the Γ point of (a) GaN and (b) AlN vs biaxial (solid line) and uniaxial (dot-dashed line) strain.

tions as well as the strain-dependent crystal-field splittings are plotted in Figs. 8(a) (GaN) and 8(b) (AlN). For comparison, the behavior in the presence of hydrostatic pressure is shown in Fig. 9. The effect of the spin-orbit splitting is not taken into account. However, its influence on the strain dependence of the various electronic energies should be negligible. The corresponding strain coefficients are derived directly from the slopes in Fig. 8 and are given in Table VI, together with the volume deformation potentials $a_V^i = (V\,\partial E_i/\partial V)_0$.

There is a completely different behavior of the A/B or C transitions versus biaxial or uniaxial strain. The C transition shows a relatively larger variation, i.e., gap shrinkage with tensile biaxial strain, than the A/B transitions, which in turn are more sensitive to uniaxial strain. As a consequence, in GaN the energetical ordering of the A/B and C transitions changes at small tensile biaxial strain (approximately 0.1%) due to the small crystal-field splitting in the strain-free case, which we obtained as $\Delta_{cr}^{GaN}(0) = 9.3$ meV. This is in good agreement with other calculations[82] and with experimental findings,[82,84] provided that the assignment of the *A*, *B*, and *C* transitions to a certain energy gap is made according to the

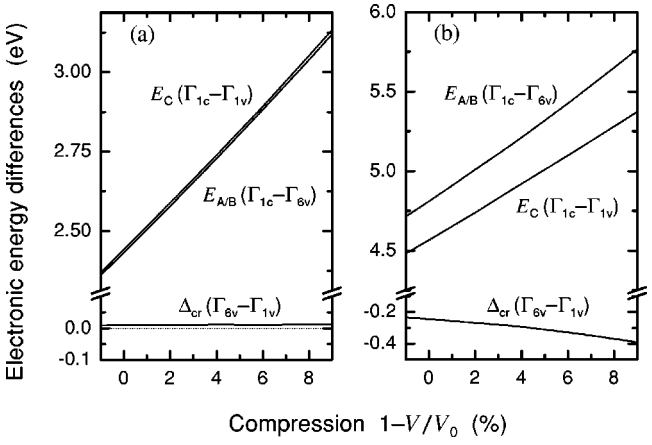

FIG. 9. As in Fig. 8 but for the case of hydrostatic pressure. The energy differences are given vs the relative volume compression. Note the different scaling of the ordinates in (a) and (b).

symmetry of the states which form the respective gap. A similar crossing of the transition energies occurs for small compressive uniaxial strain. In AlN, the C energy gap slightly increases with tensile uniaxial strain. Here the crossings are found only for large strains due to the large zero-strain value of the crystal-field splitting, which we calculated to be $\Delta_{cr}^{AlN}(0) = -244$ meV. Furthermore, it is interesting to note that in AlN the A/B transition behaves nearly identical under uniaxial and biaxial strain, whereas this is not the case for GaN.

In contrast to the transition energies, the strain behavior of the crystal-field splitting is rather similar in GaN and AlN. As pointed out by Wei and Zunger,[91] for biaxial strain Δ_{cr} mainly follows the changes of the structural parameters c/a and u, with a more sensitive dependence on the latter. Here it is found that, independent of the strain type, the crystal-field splitting decreases with increasing u and with decreasing c/a. The variation of Δ_{cr} is larger in AlN where the relative change both of u and of c/a is larger than in GaN (cf. Table II). This also holds for the case of hydrostatic compression, where u and c/a exhibit nearly no change in GaN, whereas in AlN there is a remarkable increase (decrease) of u (c/a) with rising pressure.[26]

The average values of the volume deformation potentials agree well with results of other *ab initio* calculations using the linearized muffin-tin orbital (LMTO) method.[41,83] The same conclusion holds for the hydrostatic-pressure coefficients $(\partial E_{A/B/C}/\partial p)|_{p=0} = -a_V^{A/B/C}/B_0$ given in Table VII. There are several experimental values for GaN.[86–88] The ordering of their magnitude does not correspond to that of the respective volume deformation potentials (cf. Table VI). This is due to different values of the bulk modulus used. The theoretical values tend to slightly underestimate the measured pressure coefficients. This may be related to the underestimation of the fundamental gap within the DFT-LDA. The inclusion of quasiparticle corrections should somewhat increase the absolute values of the deformation potentials.[83] The pressure dependence of the crystal-field splitting is found to be in good accordance with experiment. The value obtained from the calculation, which is the difference between the pressure coefficients of the A/B and the C gap, is 0.3 meV/GPa, and experimentally, a value of 0.4 meV/GPa is found.[87]

The pressure coefficients can also be combined from the coefficients $(\partial E_{A/B/C}/\partial \sigma_{\perp/||})|_{\boldsymbol{\sigma}=\mathbf{0}}$ per unit stress (also given in Table VII). The experimentally determined biaxial-stress coefficients deserve special attention, since in some cases, the same errors were incorporated as discussed above for the phonon coefficients. For example, in Ref. 78 two stress coefficients for the near-band-gap emission were given, which suffer from errors in the conversion factors and the conversion formula. Instead of -27 meV/GPa, the value determined from x-ray diffraction has to be -16 meV/GPa, and according to the corrected coefficient for the E_2^{high} Raman mode, the value determined from the Raman experiments has to be -9.1 meV/GPa instead of -21 meV/GPa. Further, from Ref. 78 a relation follows between the shift of the luminescence peak and the shift of the E_2^{high} Raman mode of

TABLE VI. Strain coefficients and volume deformation potentials (in eV) of the band-gap energies for biaxial and uniaxial strain as well as for hydrostatic compression, respectively, in comparison with other directly determined experimental and theoretical values. Where necessary, the factor R^B for conversion of coefficients relative to ϵ_{zz} to ones relative to ϵ_{xx} is shown. Additionally, values a_V for the average gap from the literature are also listed.

	$\frac{\partial E_{A/B}}{\partial \epsilon_\perp}$	$\frac{\partial E_C}{\partial \epsilon_\perp}$	$\frac{\partial E_{A/B}}{\partial \epsilon_\parallel}$	$\frac{\partial E_C}{\partial \epsilon_\parallel}$	$a_V^{A/B}$	a_V^C	a_V
GaN							
present	-4.85	-15.68	-9.02	-0.48	-7.21	-7.26	
calc.	-5.5[a]	-13[a]					-8,[a] -6.9,[b] -7.8[c]
exper.	-8.2,[a] -8.56,[d] -9.22[e]	-13,[a]					-8.8,[f] -8.9,[g] -9.2[h]
	-8.7,[i] -7.2[j], -9.4[k]	-17.24[d]					
	$-12R^B(-6.4)$[l]						
	$-17R^B(-9)$[m]						
AlN							
present	-7.73	-21.58	-9.50	1.58	-9.70	-8.60	
calc.							-9.0,[b] -8.8[c]

[a]Reference 82 (for the biaxial strain coefficient of the crystal-field splitting, a calculated value of -9 eV is mentioned, however, it does not fit to the two values for the gaps).
[b]Reference 41.
[c]Reference 83.
[d]Reference 84.
[e]Reference 85.
[f]Reference 86.
[g]Reference 87.
[h]Reference 88.
[i]Reference 89.
[j]Reference 90.
[k]Reference 7.
[l]Reference 64.
[m]Reference 12.

24.4 meV/7.4 $cm^{-1}=3.3\times10^{-3}$ eV cm. In contrast, in Ref. 12 a value of 6.6×10^{-3} eV cm was reported. The latter paper gave a value for the biaxial-stress coefficient of -27 meV/GPa, which has to be corrected for the used elastic moduli to end up at -19 meV/GPa. This seems to be quite a reasonable value, since similar values, which are free from the above-mentioned errors, are reported in two other studies.[7,89] Nevertheless, we have to conclude that the stress coefficient calculated for the A/B transition in GaN is too low. On the other hand, the corrected values of the stress coefficients also show that, by using a luminescence shift, the stress which accompanies the biaxial strain might have been underestimated so far.

The deformation potentials of the *A*, *B*, and *C* electronic transitions are listed in Table VIII. As mentioned in Sec. II D, our results were obtained from calculations for ''artificial'' deformations. The agreement with the results of another first-principles calculation based on pseudopotentials[66] is excellent for both GaN and AlN. This holds in particular for the deformation potentials of the crystal-field splitting but also for the deformation potentials that apply to strain in the plane perpendicular to the *c* axis. The values obtained within a full-potential linearized-augmented-plane-wave method[93,94] show the correct trend. However, the absolute values are different. This may be partly due to the elastic constants that have been used, since in a previous paper, where different ones were chosen, the obtained deformation potentials were larger.[92] In the latter paper, however, it seems that the values for b_1 and b_2 were interchanged. Much better agreement is obtained with a FP-LMTO[95] and a first-principles pseudopotential calculation.[39] Unfortunately, the comparison with the majority of the calculations is incomplete since only the deformation potentials D_1–D_4 for the valence bands are given and not those for the conduction band. Therefore, no comment can be made concerning the transition-related deformation potentials.

The so-called quasicubic approximation for the electronic deformation potentials is defined by the relations $b_1 \approx -2b_2$ and $a_2-a_1\approx b_1$. We find that the first relation is valid for GaN and not too bad for AlN, but the second one does not hold for GaN at all, whereas for AlN it is still reasonable. This conclusion is confirmed by the results of the calculation presented in Ref. 66. The approximate validity of the quasicubic approximation in the AlN case is surprising, since for the other properties studied, it has been found to be the more anisotropic material. Conversely, in the GaN case it was not expected that the second relation is not applicable. The reason for this is that the deformation potentials describe the strain-related *changes* of the electronic band structure, which are not necessarily related to the latter in the unstrained case. Rather, the strain brings about significant changes in the atomic geometry. Strong deformations of the bonding tetrahedra may induce remarkable deviations from the quasicubic character of the electronic states.

For a comparison with measured data one should bear in mind that the experimental extraction of the deformation potentials, in addition to the use of certain assumptions, requires a knowledge of many parameters, especially about the

TABLE VII. Stress and pressure coefficients (in meV/GPa) which give the gap changes for biaxial and uniaxial stress as well as for hydrostatic pressure, respectively. The values in parentheses are recalculated in order to adjust for deviating formulas and/or values of the elastic stiffness constants. For comparison values for the average gap from the literature are also listed.

	$\frac{\partial E_{A/B}}{\partial \sigma_\perp}$	$\frac{\partial E_C}{\partial \sigma_\perp}$	$\frac{\partial E_{A/B}}{\partial \sigma_\parallel}$	$\frac{\partial E_C}{\partial \sigma_\parallel}$	$\frac{\partial E_{A/B}}{\partial p}$	$\frac{\partial E_C}{\partial p}$	$\frac{\partial E_g}{\partial p}$
GaN							
present	−10.5	−33.9	−24.2	−1.29	34.8	35.1	
calc.							33,[a] 39[b]
exper.	−27 (−19)[c]						44,[d] 43,[e]
	−27 (−16)[f]						39[g]
	−21 (−9)[h]						
	−20,[i] −19[j]						
AlN							
present	−16.5	−46.0	−29.5	4.9	46.2	41.0	
calc.							44,[a] 40[b]

[a]Reference 41.
[b]Reference 83.
[c]Reference 12.
[d]Reference 86.
[e]Reference 87.
[f]Reference 78, strain determination from x-ray measurements.
[g]Reference 88.
[h]Reference 78, strain determination from Raman measurements.
[i]Reference 7.
[j]Reference 89.

sample quality, the band structure close to the band gap, and the homogeneity of the strain. Also the elastic constants and reference values for the stress-free lattice constants, which are required for the determination of the strain, play a crucial role, as discussed above. Furthermore, in many cases an evaluation of the deformation potentials is possible only under additional assumptions. Usually, a homogeneous biaxial strain is assumed in the GaN layer, and the quasicubic approximation for the deformation potentials is used. The latter holds for the results of Refs. 6,37,84,85, and 97–99. The data of Ref. 96 were obtained by assuming $a_1=a_2=a_V$. The latter results were used both in Ref. 6 (with the additional assumption of $a_{cx}=a_{cz}=a_V/2$) and in Ref. 97 (carefully discussing the influence of the different sets of elastic constants on the results). In Ref. 98, findings of Refs. 85 (experimental) and 93 (calculated) have been used for the derivation of the results. The reinterpreted data of Refs. 6 and 97 show a more realistic trend than the original ones. The agreement with some of the experimental deformation potentials for GaN is reasonable,[37,97,98] except for the case of a_2, which is somewhat larger in the experiment. This might be due to the utilization of the quasicubic approximation. In part, the absolute values of the deformation potentials referring to the crystal-field splittings, b_1 and b_2, are somewhat overestimated by the theory; the agreement with the more recent results[84,85,99] is, however, rather good.

From the deformation potentials, also the strain coefficients can again be obtained. This is particularly interesting in those cases where these values have not been given explicitly. One has $\partial E_{A/B}/\partial \epsilon_\perp = -R^B(a_1+b_1)+2(a_2+b_2)$ and $\partial E_C/\partial \epsilon_\perp = -R^B a_1 + 2a_2$. The resulting values are also listed in in Table VIII. A comparison with Table VI shows that our results, which were obtained from independent calculations, completely agree with each other. Only for GaN are experimental values available. The agreement with the calculated results is less satisfying than it was for the deformation potentials. In general, there is a tendency for some underestimation of the experimental results by the electronic-structure calculations. On the other hand, in comparison with the data given in Table VI, the experimental strain coefficients also show discrepancies among themselves.

IV. SUMMARY

In summary, we have used *ab initio* density-functional calculations to investigate structural, elastic, dielectric, vibrational, and electronic properties of strained GaN and AlN wurtzite crystals. The space-group-conserving biaxial and uniaxial strains parallel to the *c* axis have been studied. We observed that biaxial and uniaxial strains induce qualitatively similar changes of the bond lengths. Nevertheless, the internal strain and the bond angles are found to exhibit opposite tendencies with the two different strains. For slightly compressive biaxial strain, on the one hand, and for slightly tensile uniaxial strain, on the other hand, we observed a tendency for realization of bond angles corresponding to ideal tetrahedra.

The different elastic behavior of GaN (quasicubic) and AlN (anisotropic), as previously found under hydrostatic pressure, also follows from a comparison of the biaxial and uniaxial strain-relaxation coefficients R^B and ν. Conversely, we demonstrated that the known physical behavior of an

TABLE VIII. Deformation potentials of the A,B, and C transition energies (in eV). For comparison, the resulting biaxial strain coefficients are also given. They are obtained using the following values for R^B: For the calculated ones, the respective theoretical result is used, but for all experimental ones, again the result of Polian *et al.* (Ref. 44) is employed. In addition, the zero-strain value of the crystal-field splitting (in meV) is also shown.

	a_1	a_2	b_1	b_2	$\Delta_{cr}(0)$	$\frac{\partial E_{A/B}}{\partial \epsilon_\perp}$	$\frac{\partial E_C}{\partial \epsilon_\perp}$
GaN							
present	−4.09	−8.87	−7.02	3.65	9.3	−4.86	−15.69
calc.[a]	−5.55	−9.38	−6.61	3.55	35.3	−6.11	−16.23
calc.[b]			−2.92	5.84	72.9		
calc.[c]			−3.03	1.52	72.9		
calc.[d]			−2.99	1.63	72.1		
calc.[e]			−5.7	2.85	36		
calc.[f]			−5.80	3.25	50.4		
exper.[g]	−6.5	−11.8	−5.3	2.7		−11.9	−20.1
exper.[h]	−8.16	−8.16	−1.44	0.72	10.0	−9.76	−11.97
exper.[i]	−4.78	−6.18	−1.4	0.7	16	−7.67	−9.81
exper.[j]	−5.32	−10.23	−4.91	2.46	10.0	−10.09	−17.62
exper.[k]			−5.73	2.86	21		
exper.[l]			−8.82	4.41	22		
exper.[m]	−3.1	−11.2	−8.2	4.1	22	−8.18	−20.75
exper.[n]			−7.2	3.6	10		
AlN							
present	−3.39	−11.81	−9.42	4.02	−244	−7.75	−21.55
calc.[a]	−4.38	−12.48	−9.18	4.10	−211	−9.01	−22.46
calc.[c]			−4.46	2.23	−58.5		
calc.[d]			−4.76	2.04	−58.5		
calc.[e]			−9.6	4.8	−215		
calc.[f]			−8.84	3.92	−176		

[a]Reference 66 (the original data of this paper refer to the center of gravity of the valence bands and have been recalculated).
[b]Reference 92.
[c]Reference 93.
[d]Reference 94.
[e]Reference 95.
[f]Reference 39.
[g]Reference 37 (in this paper, only a value for a combination of $\Delta_{cr}(0)$ with spin-orbit-splitting parameters is given).
[h]Reference 96.
[i]Reference 6.
[j]Reference 97.
[k]Reference 84.
[l]Reference 85.
[m]Reference 98.
[n]Reference 99.

elastic material (here: of GaN and AlN) under hydrostatic pressure can be used as a test for the reliability of its elastic stiffness constants.

The linear strain coefficients of the dielectric constants and dynamic charges are similar for biaxial and uniaxial strain, at least from a qualitative point of view. A somewhat contrary behavior is shown by the xx (zz) component of the Born charge tensor of GaN (AlN) and the zz component of the static dielectric constant of AlN versus the uniaxial strain. We stated an enhanced anisotropy of the static dielectric constants compared with the high-frequency ones and a rather large sensitivity of the static dielectric constants with respect to the biaxial strain.

The strain dependences of the zone-center phonon frequencies are rather similar for all mode symmetries and independent of the group-III atom. However, the mode frequencies are much more sensitive to biaxial strain than to uniaxial one. The strain coefficients differ practically by a factor of 2. The only exception is represented by the lower E_2 modes. A mode softening has been observed for biaxial strain, while the lower E_2 modes exhibit a ''normal'' behavior under uniaxial deformation, although the absolute changes are small. Furthermore, the phonon frequency shifts were described on the basis of a decomposition into contributions stemming from an isotropic and a shear strain. The corresponding deformation potentials show significant differences between GaN and AlN. The unusual behavior of the lower E_2 modes of both GaN and AlN as well as that of the

lower B_1 and the $A_1(\mathrm{TO})$ mode of AlN has been discussed in terms of only these two contributions.

The comparison of the calculated biaxial strain coefficients of the zone-center phonon frequencies of GaN with measured values shows reasonable agreement, whereas for the stress coefficients this holds only after a recalculation of the experimental data. In many cases, the latter have to be corrected for the elastic stiffness constants and conversion formulas employed. We noted that an appropriate definition of the strain-free situation is important as well. The recalculated coefficients give a reliable basis for a characterization of the strain and/or stress stage of GaN and AlN layers just by measuring the shift of the Raman frequencies. We pointed out that, since the biaxial stress coefficients are smaller than previously reported, up to now the accompanying stress has been underestimated.

The fundamental optical transitions at the absorption edge of the wurtzite group-III nitrides are $\Gamma_{6v}\rightarrow\Gamma_{1c}$ (A/B) and $\Gamma_{1v}\rightarrow\Gamma_{1c}$ (C). In general, their energies show the same tendency versus biaxial or uniaxial strain: There is a gap widening for compressive strain and, hence, a gap shrinkage for tensile strain. However, the degree of the gap changes, i.e., the strain coefficient, depends strongly on the transition and the strain type. In AlN the A/B transition behaves nearly identical under uniaxial and biaxial strain, whereas this is not the case for GaN. In general, the C transition gap is rather insensitive to the applied uniaxial strain, but exhibits the strongest variations in the case of biaxial strain. More or less the opposite effect happens for the A/B transitions. The reason for this is the opposite behavior of the crystal-field splitting versus biaxial or uniaxial strain. This opposite behavior represents the different dependence of the Γ_{6v} and Γ_{1v} levels on increasing the c/a ratio and the u parameter. We found that the electronic interband deformation potentials of GaN do not fulfill the widely used quasicubic approximation instead the latter holds for AlN, in contrast to their opposite elastic behavior.

Note added in proof. Recently, our attention was brought to an experimental result by Sarua *et al.* who found a phonon frequency shift of 3 cm^{-1}/GPa for the E_2^{high} mode of AlN under biaxial stress.[100]

ACKNOWLEDGMENTS

This work was supported by the Deutsche Forschungsgemeinschaft (Schwerpunktprogramm ''Gruppe-III-Nitride,'' Contract No. Be 1346/8-5). The computations were performed at the John von Neumann Center for Computing in Jülich.

[1] H. Morkoç, S. Strite, G.B. Gao, M.E. Lin, B. Sverdlov, and M. Burns, J. Appl. Phys. **76**, 1363 (1994).
[2] W.G. Perry, T. Zheleva, M.D. Bremser, R.F. Davies, W. Shan, and J.J. Song, J. Electron. Mater. **26**, 224 (1997).
[3] S.C. Jain, M. Willander, J. Narayan, and R. Van Overstraeten, J. Appl. Phys. **87**, 965 (2000).
[4] G. Steude, B.K. Meyer, A. Göldner, A. Hoffmann, F. Bechstedt, H. Amano, and I. Akasaki, Jpn. J. Appl. Phys. **38**, L498 (1999).
[5] J. Gleize, F. Demangeot, J. Frandon, M.A. Renucci, F. Widmann, and B. Daudin, Appl. Phys. Lett. **74**, 703 (1999).
[6] S.L. Chuang and C.S. Chang, Phys. Rev. B **54**, 2491 (1996).
[7] V.Yu. Davydov, N.S. Averkiev, I.N. Goncharuk, D.K. Nelson, I.P. Nikitina, A.S. Polkovnikov, A.N. Smirnov, M.A. Jacobson, and O.K. Semchinova, J. Appl. Phys. **82**, 5097 (1997).
[8] B. Jogai, Phys. Rev. B **57**, 2382 (1998).
[9] S.-H. Park and S.-L. Chuang, Phys. Rev. B **59**, 4725 (1999).
[10] B.C. Lee, K.W. Kim, M. Dutta, and M.A. Stroscio, Phys. Rev. B **56**, 997 (1997); B.C. Lee, K.W. Kim, M.A. Stroscio, and M. Dutta, *ibid.* **58**, 4860 (1998).
[11] F. Demangeot, J. Frandon, M.A. Renucci, O. Briot, B. Gil, and R.L. Aulombard, Solid State Commun. **100**, 207 (1996); MRS Internet J. Nitride Semicond. Res. **1**, 23 (1996).
[12] C. Kisielowski, J. Krüger, S. Ruvimov, T. Suski, J.W. Ager, III, E. Jones, Z. Liliental-Weber, M. Rubin, E.R. Weber, M.D. Bremser, and R.F. Davis, Phys. Rev. B **54**, 17 745 (1996).
[13] M. Klose, N. Wieser, G.C. Rohr, R. Dassow, F. Scholz, and J. Off, J. Cryst. Growth **189/190**, 634 (1998).
[14] J. W. Ager III, G. Conti, L. T. Romano, and C. Kisielowski, in *Nitride Semiconducters*, edited by F. A. Ponve, S. P. Den Baars, B. K. Meyer, S. Nakamura, and S. Strite, MRS Symposia Proceedings No. **482**, (Materials Research Society, Pittsburgh, 1998), p. 769.
[15] T. Prokofyeva, M. Seon, J. Vanbuskirk, M. Holtz, S.A. Nikishin, N.N. Faleev, H. Temkin, and S. Zollner, Phys. Rev. B **63**, 125313 (2001).
[16] N. Wieser, M. Klose, R. Dassow, G.C. Rohr, F. Scholz, and J. Off, Mater. Sci. Eng., B **50**, 88 (1997).
[17] J. Gleize, F. Demangeot, J. Frandon, M.A. Renucci, M. Kuball, F. Semond, and J. Massies, Phys. Status Solidi A **188**, 511 (2001).
[18] J. W. Ager III, T. Suski, S. Ruvimov, J. Krüger, G. Conti, E. R. Weber, M. D. Bremser, R. Davis, and C. P. Kuo, in *III-V Nitrides*, edited by F. A. Ponce, T. D. Moustakas, I. Akasaki, and B. A. Monemar, MRS Symposia Proceedings No. **449**, (Materials Research Society, Pittsburgh, 1997), p. 775.
[19] K. Karch and F. Bechstedt, Phys. Rev. B **56**, 7404 (1997); K. Karch, F. Bechstedt, and T. Pletl, *ibid.* **56**, 3560 (1997).
[20] K. Karch, J.-M. Wagner, and F. Bechstedt, Phys. Rev. B **57**, 7043 (1998).
[21] P. Perdew and A. Zunger, Phys. Rev. B **23**, 5048 (1981).
[22] N. Troullier and J.L. Martins, Phys. Rev. B **43**, 1993 (1991).
[23] S.G. Louie, S. Froyen, and M.L. Cohen, Phys. Rev. B **26**, 1738 (1982).
[24] D.J. Chadi and M.L. Cohen, Phys. Rev. B **8**, 5747 (1973).
[25] J. F. Nye, *Physical Properties of Crystals* (Oxford University Press, Oxford, 1985).
[26] J.-M. Wagner and F. Bechstedt, Phys. Rev. B **62**, 4526 (2000).
[27] P. Vinet, J. Ferrante, J.R. Smith, and J.H. Rose, J. Phys. C **19**, L467 (1986).
[28] P. Giannozzi, S. de Gironcoli, P. Pavone, and S. Baroni, Phys. Rev. B **43**, 7231 (1991).

[29] W. Cochran and R.H. Cowley, J. Phys. Chem. Solids **23**, 447 (1962).
[30] G. Venkataraman, L. A. Feldkamp, and V. C. Sahni, *Dynamics of Perfect Crystals* (MIT Press, Cambridge, MA, 1975).
[31] A. Gavini and M. Cardona, Phys. Rev. B **1**, 672 (1970).
[32] R.J. Briggs and A.K. Ramdas, Phys. Rev. B **13**, 5518 (1976).
[33] E. Anastassakis, Acta Physica Hung. **74**, 83 (1994).
[34] J.-M. Wagner and F. Bechstedt, Appl. Phys. Lett. **77**, 346 (2000).
[35] H. Yamashita, K. Fukui, S. Misawa, and S. Yoshida, J. Appl. Phys. **50**, 896 (1979).
[36] A. Rubio, J.L. Corkill, M.L. Cohen, E.L. Shirley, and S.G. Louie, Phys. Rev. B **48**, 11 810 (1993).
[37] W. Shan, R.J. Hauenstein, A.J. Fischer, J.J. Song, W.G. Perry, M.D. Bremser, R.F. Davis, and B. Goldenberg, Phys. Rev. B **54**, 13 460 (1996).
[38] A.F. Wright, J. Appl. Phys. **82**, 2833 (1997).
[39] K. Shimada, T. Sota, and K. Suzuki, J. Appl. Phys. **84**, 4951 (1998).
[40] E. Ruiz, S. Alvarez, and P. Alemany, Phys. Rev. B **49**, 7115 (1994).
[41] K. Kim, W.R.L. Lambrecht, and B. Segall, Phys. Rev. B **53**, 16 310 (1996).
[42] K. Kim, W.R.L. Lambrecht, and B. Segall, Phys. Rev. B **50**, 1502 (1994).
[43] R. Kato and J. Hama, J. Phys.: Condens. Matter **6**, 7617 (1994).
[44] A. Polian, M. Grimsditch, and I. Grzegory, J. Appl. Phys. **79**, 3343 (1996).
[45] L.E. McNeil, M. Grimsditch, and R.H. French, J. Am. Ceram. Soc. **76**, 1132 (1993).
[46] C. Deger, E. Born, H. Angerer, O. Ambacher, M. Stutzmann, J. Hornsteiner, E. Riha, and G. Fischerauer, Appl. Phys. Lett. **72**, 2400 (1998).
[47] M. Yamaguchi, T. Yagi, T. Azuhata, T. Sota, K. Suzuki, S. Chichibu, and S. Nakamura, J. Phys.: Condens. Matter **9**, 241 (1997).
[48] M. Yamaguchi, T. Yagi, T. Sota, T. Deguchi, K. Shimada, and S. Nakamura, J. Appl. Phys. **85**, 8502 (1999).
[49] R.R. Reeber and K. Wang, MRS Internet J. Nitride Semicond. Res. **6**, 3 (2001).
[50] S.Yu. Davydov and A.V. Solomonov, Pis'ma Zh. Tekh. Fiz. **25**, 23 (1999) [Tech. Phys. Lett. **25**, 601 (1999)].
[51] V.Yu. Davydov, Yu.E. Kitaev, I.N. Goncharuk, A.N. Smirnov, J. Graul, O. Semchinova, D. Uffmann, M.B. Smirnov, A.P. Mirgorodsky, and R.A. Evarestov, Phys. Rev. B **58**, 12 899 (1998).
[52] K. Tsubouchi and N. Mikoshiba, IEEE Trans. Sonics Ultrason. **SU-32**, 634 (1985).
[53] V.A. Savastenko and A.U. Sheleg, Phys. Status Solidi A **48**, K135 (1978).
[54] R.B. Schwarz, K. Khachaturyan, and E.R. Weber, Appl. Phys. Lett. **70**, 1122 (1997).
[55] T. Deguchi, D. Ichiryu, K. Toshikawa, K. Sekiguchi, T. Sota, R. Matsuo, T. Azuhata, M. Yamaguchi, T. Yagi, S. Chichibu, and S. Nakamura, J. Appl. Phys. **86**, 1860 (1999).
[56] M. Ueno, A. Onodera, O. Shimomura, and K. Takemura, Phys. Rev. B **45**, 10 123 (1992).
[57] M. Ueno, M. Yoshida, A. Onodera, O. Shimomura, and K. Takemura, Phys. Rev. B **49**, 14 (1994).
[58] N.E. Christensen and I. Gorczyca, Phys. Rev. B **47**, 4307 (1993).
[59] J. Serrano, A. Rubio, E. Hernández, A. Muñoz, and A. Mujica, Phys. Rev. B **62**, 16 612 (2000).
[60] W. Shan, A.J. Fischer, S.J. Hwang, B.D. Little, R.J. Hauenstein, X.C. Xie, J.J. Song, D.S. Kim, B. Goldenberg, R. Horning, S. Krishnankutty, W.G. Perry, M.D. Bremser, and R.F. Davis, J. Appl. Phys. **83**, 455 (1998).
[61] S. Yamaguchi, M. Kariya, T. Kashima, S. Nitta, M. Kosaki, Y. Yukawa, H. Amano, and I. Akasaki, Phys. Rev. B **64**, 035318 (2001).
[62] T. Detchprohm, K. Hiramatsu, K. Itoh, and I. Aksaki, Jpn. J. Appl. Phys. **31**, L1454 (1992).
[63] L.T. Romano, C.G. Van de Walle, J.W. Ager III, W. Götz, and R.S. Kern, J. Appl. Phys. **87**, 7745 (2000).
[64] H. Amano, K. Hiramatsu, and I. Akasaki, Jpn. J. Appl. Phys. **27**, L1384 (1988).
[65] M. Leszczynski, H. Teisseyre, T. Suski, I. Grzegory, M. Bockowski, J. Jun, S. Porowski, K. Pakuła, J.M. Baranowski, C.T. Foxon, and T.S. Cheng, Appl. Phys. Lett. **69**, 73 (1996).
[66] J.A. Majewski, M. Städele, and P. Vogl, MRS Internet J. Nitride Semicond. Res. **1**, 30 (1996).
[67] A. Zoroddu, F. Bernardini, P. Ruggerone, and V. Fiorentini, Phys. Rev. B **64**, 045208 (2001).
[68] O. Lagerstedt and B. Monemar, Phys. Rev. B **19**, 3064 (1979).
[69] A.S. Barker and M. Ilegems, Phys. Rev. B **7**, 743 (1973).
[70] T. Azuhata, T. Sota, K. Suzuki, and S. Nakamura, J. Phys.: Condens. Matter **7**, L129 (1995).
[71] F. Malengreau, M. Vermeersch, S. Hagège, R. Sporken, M.D. Lange, and R. Caudano, J. Mater. Res. **12**, 175 (1997).
[72] A.N. Pikhtin and A.D. Yas'kov, Fiz. Tekh. Poluprovodn. **15**, 15 (1981) [Sov. Phys. Semicond. **15**, 8 (1981)].
[73] I. Akasaki and M. Hashimoto, Solid State Commun. **5**, 851 (1967).
[74] G. Yu, H. Ishikawa, T. Egawa, T. Soga, J. Watanabe, T. Jimbo, and M. Umeno, Jpn. J. Appl. Phys. **36**, L1029 (1997).
[75] D.J. Jones, R.H. French, H. Müllejans, S. Loughin, A.D. Dorneich, and P.F. Carcia, J. Mater. Res. **14**, 4337 (1999).
[76] N. Wieser, Ph.D. Thesis (Technische Universität München, 2000); and (private communication).
[77] A.R. Goñi, H. Siegle, K. Syassen, C. Thomsen, and J.-M. Wagner, Phys. Rev. B **64**, 035205 (2001).
[78] W. Rieger, T. Metzger, H. Angerer, R. Dimitrov, O. Ambacher, and M. Stutzmann, Appl. Phys. Lett. **68**, 970 (1996).
[79] W. Voigt, *Lehrbuch der Kristallphysik* (Teubner, Leipzig, 1910), p. 962f.
[80] M. Giehler, M. Ramsteiner, P. Waltereit, K.H. Ploog, and H. Obloh, J. Appl. Phys. **89**, 3634 (2001).
[81] P. Perlin, C. Jauberthie-Carillon, J.P. Itie, A. San Miguel, I. Grzegory, and A. Polian, Phys. Rev. B **45**, 83 (1992).
[82] D. Volm, K. Oettinger, T. Streibl, D. Kovalev, M. Ben-Chorin, J. Diener, B.K. Meyer, J. Majewski, L. Eckey, A. Hoffmann, H. Amano, I. Akasaki, K. Hiramatsu, and T. Detchprohm, Phys. Rev. B **53**, 16 543 (1996).
[83] N.E. Christensen and I. Gorczyca, Phys. Rev. B **50**, 4397 (1994).
[84] S. Chichibu, A. Shikanai, T. Azuhata, T. Sota, A. Kuramata, K. Horino, and S. Nakamura, Appl. Phys. Lett. **68**, 3766 (1996).
[85] A. Shikanai, T. Azuhata, T. Sota, S. Chichibu, A. Kuramata, K. Horino, and S. Nakamura, J. Appl. Phys. **81**, 417 (1997).
[86] K. Reimann, M. Steube, O. Brandt, H. Yang, and K.H. Ploog, J. Appl. Phys. **84**, 2971 (1998).
[87] Z.X. Liu, K.P. Korona, K. Syassen, J. Kuhl, K. Pakuła, J.M. Bara-

nowski, I. Grzegory, and S. Porowski, Solid State Commun. **108**, 433 (1998).
[88] W. Shan, T.J. Schmidt, R.J. Hauenstein, J.J. Song, and B. Goldenberg, Appl. Phys. Lett. **66**, 3489 (1995).
[89] A. Cremades, L. Görgens, O. Ambacher, M. Stutzmann, and F. Scholz, Phys. Rev. B **61**, 2812 (2000).
[90] S. Yamaguchi, M. Kariya, M. Kosaki, Y. Yukawa, S. Nitta, H. Amano, and I. Akasaki, J. Appl. Phys. **89**, 7820 (2001).
[91] S.-H. Wei and A. Zunger, Appl. Phys. Lett. **69**, 2719 (1996).
[92] S. Kamiyama, K. Ohnaka, M. Suzuki, and T. Uenoyama, Jpn. J. Appl. Phys. **34**, L821 (1995).
[93] M. Suzuki and T. Uenoyama, Jpn. J. Appl. Phys. **35**, 1420 (1996).
[94] M. Suzuki and T. Uenoyama, J. Appl. Phys. **80**, 6868 (1996).
[95] K. Kim, W.R.L. Lambrecht, B. Segall, and M. van Schilfgaarde, Phys. Rev. B **56**, 7363 (1997).
[96] M. Tchounkeu, O. Briot, B. Gil, J.P. Alexis, and R.-L. Aulombard, J. Appl. Phys. **80**, 5352 (1996); B. Gil, O. Briot, and R.-L. Aulombard, Phys. Rev. B **52**, R17 028 (1995).
[97] B. Gil and A. Alemu, Phys. Rev. B **56**, 12 446 (1997).
[98] S. Ghosh, P. Waltereit, O. Brandt, H.T. Grahn, and K.H. Ploog, Phys. Rev. B **65**, 075202 (2002).
[99] A.A. Yamaguchi, Y. Mochizuki, H. Sunakawa, and A. Usui, J. Appl. Phys. **83**, 4542 (1998).
[100] A. Sarua, M. Kuball, and J. E. Van Nostrand, Appl. Phys. Lett. **81**, 1426 (2002)].